

Photon Management in Silicon Photovoltaic Cells: A Critical Review

Mohammad Jobayer Hossain^{1,5,6,*}, Mengdi Sun^{1,7}, Kristopher O. Davis^{1,2,3,4}

¹CREOL, the College of Optics and Photonics, University of Central Florida, Orlando, Florida, USA

²Resilient Intelligent Sustainable Energy Systems (RISES) Faculty Cluster, University of Central Florida, Orlando, Florida, USA

³Department of Materials Science and Engineering, University of Central Florida, Orlando, Florida, USA

⁴FSEC Energy Research Center, Cocoa, Florida, USA

⁵American Institute for Manufacturing Integrated Photonics (AIM Photonics), Albany, New York, USA

⁶The Research Foundation for State University of New York, Albany, New York, USA

⁷Bradley Department of Electrical and Computer Engineering, Virginia Tech, Arlington, Virginia, USA

*Corresponding author: jobayer@knights.ucf.edu

Abstract

With the practical efficiency of the silicon photovoltaic (PV) cell approaching its theoretical limit, pushing conversion efficiencies even higher now relies on reducing every type of power loss that can occur within the device. Limiting optical losses is therefore critical and requires effective management of incident photons in terms of how they interact with the device. Ultimately, photon management within a PV cell means engineering the device and constituent materials to maximize photon absorption within the active semiconductor and therefore reduce the number of photons lost through other means, most notably reflection and parasitic absorption. There have been great advancements in the front and the rear side photon management techniques in recent years. This review aims to discuss these advancements and compare the various approaches, not only in terms of increases in photogenerated current, but also their compatibility with different PV cell architectures and potential trade-offs, like increased surface recombination or scalability for high-volume manufacturing. In this review, a comprehensive discussion of a wide variety of the front and the rear side photon management structures are presented with suggestions to improve the already achieved performance further. This review is unique because it not only presents the recent development in photon management techniques, but also offer through analysis of these techniques and pathways to improve further.

Keywords: Light trapping, path length enhancement, photon management, recombination, silicon, PV cell

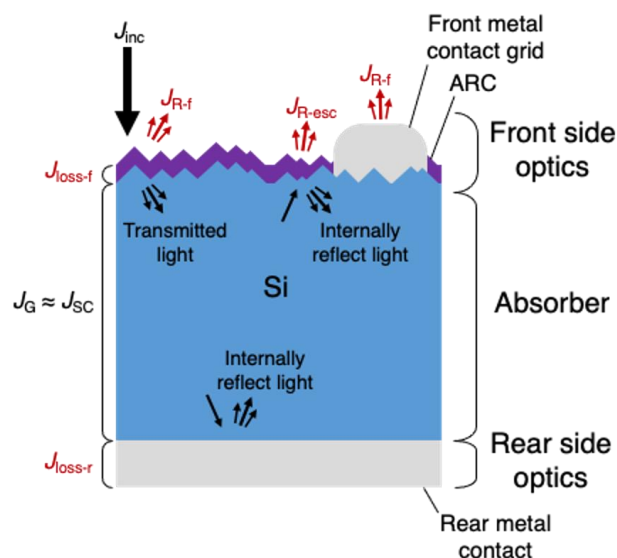


Figure 1: Simplified illustration of the light propagation in a silicon photovoltaic cell. The figure highlights the losses in red color, including reflection and absorption losses. The legend provides a breakdown of these losses, including loss in current density due to front reflectance (J_{R-f}), loss in current density due to escape reflectance (J_{R-esc}), loss in current density (absorption) at the front side (J_{loss-f}), and loss in current density (absorption) at the rear side (J_{loss-r}). This visualization provides valuable insights into the mechanisms that affect the efficiency of the photovoltaic cell, helping to identify areas for optimization and improvement.

1. Introduction

Photovoltaic (PV) energy conversion has now become one of the cheapest sources of electricity [1], less expensive than most fossil fuel-based resources. Sunlight is abundant on earth, and PV cells and modules directly convert incident photons into electricity using a process called photovoltaic effect. A wide variety of materials can be used to make PV cells, including organic semiconductors, perovskites, III-V semiconductors, chalcogenides, and of course silicon (Si). Even though some of these materials are less expensive to produce and others yield higher conversion efficiencies, Si has been and continues to dominate the PV manufacturing sector with a current market share of approximately 95% [2]. Si has a bandgap of 1.12 eV, which is an optimal value for a single junction PV cell based on the AM 1.5G solar spectrum. However, it has an indirect bandgap that results in weak absorption near the band edge. Other materials have direct bandgaps of a similar magnitude, so why does silicon remain the dominant material? For starters, Si is the second most abundant element on earth, behind only oxygen. Secondly, many decades worth of research, development, and production in the integrated circuits sector have led to an incredible understanding of how to work with Si and produce it at a large scale. Finally, Si-based modules have shown to be very durable and reliable over time with very low degradation rates reported from the field [3–6]. This, combined with the relatively high efficiencies obtained and the low production costs, have all contributed to the continued use of Si by PV manufacturers.

Incident photons coming from the sun serve as the “fuel source” in a PV cell. The wavelengths of these photons span the ultraviolet, visible, and infrared domains. Not all the incident photons enter the cell. As illustrated in Fig. 1, some are reflected off the front surface of the cell and others are parasitically absorbed by other front surface layers of the device. Of the photons that do enter the semiconductor, not all will get absorbed and generate an electron-hole pair. Photons with energies smaller than the bandgap either don’t get absorbed at all or get absorbed and converted into heat (e.g.,

free carrier absorption). Others may reach the rear side of the cell and get transmitted through the device or absorbed by other rear surface layers (e.g., metal contacts). Even photons that are internally reflected at the rear surface can escape out the front. Some of these losses associated with the rear side of the cell could be addressed by making the Si substrate much thicker, but cost constraints prevent, and to a lesser extent bulk carrier recombination, prevent the use of very thick wafers.

The efficiency of a PV cell is now one of the driving factors that governs the levelized cost of energy (LCOE). Cell manufacturing costs have gotten so low that a larger fraction of the total PV system costs can now be attributed to things like the glass and aluminum needed to make the modules, the mounting hardware, the wiring and conduit, and the installation labor. Many of these factors scale with area, so an increase in cell efficiency can yield a lower cost per watt at the system level [7]. The current world record for silicon PV cell efficiency is 26.8% [8, 9] using a heterojunction structure, while the theoretical limit of such a cell, known as the Shockley-Queisser limit, is approximately 30% [10] under AM 1.5G solar spectrum. By implementing photon management techniques and minimizing losses such as recombination, resistive and reflection losses, the gap between the current efficiency levels and the Shockley-Queisser limit can be significantly reduced.

Recent advancements in photon management techniques for Si PV cells have led to improved theoretical understanding, fabrication methods, and cost reduction. These designs range from nano-texturizing the active material to using resonators of various materials for front-side light trapping, and diffraction grating, planar metallic and dielectric layers for the rear side. These methods effectively trap light, resulting in an increase in photogenerated current density. However, these structures often come with drawbacks such as high surface recombination loss, which leads to low open-circuit voltage and fill factor, complex fabrication processes, higher contact resistivity and additional implementation costs, making them less suitable for industrial PV cell manufacturing. While many of these novel designs show promise in terms of photogenerated current density only, other performance parameters have yet to be fully explored.

Recent advancements in light trapping structures have led to a growing need for a comprehensive review of photon management in silicon PV cells within the research community. In our search for such papers, we have found several review papers on the topic, including those focusing on nanoscale photon management in silicon PV [11–13], nanostructured silicon PV [14], and thin silicon PV cells [15]. While these papers provide thorough analysis of different structures, they lack an examination of the various loss mechanisms and implementation feasibility associated with these structures. Additionally, many of these articles only focus on photon management from one side of the cell, either the front or rear. In this article, we aim to provide a comprehensive review of existing photon management schemes, with a particular emphasis on both the front and rear sides of the cell.

Silicon PV cells are diverse both in terms of how they are designed and manufactured [16–19]. This variety takes the form of different cell architectures, etching and surface preparation processes (e.g., anisotropic wet texturing [20–22], isotropic wet texturing [23–26], surface cleaning [27–33]), doping processes [34–39], materials and deposition methods for passivation layers and optical coatings [40–45], and various metallization materials and manufacturing processes [46–54]. The major cell architectures include: aluminum back surface field (Al-BSF) cells [55, 56], the dominant architecture until recently; passivated emitter rear contact (PERC) cells [57–61], the newly emerged dominant architecture; silicon heterojunctions (SHJ) or heterojunction with intrinsic thin-layer (HIT) cells [62–67], a high efficiency technology that has a smaller market share due to higher manufacturing costs; and polysilicon-based passivating contact cells, a concept introduced many years ago [68], but recently attracting a lot of attention and

development under the name of polycrystalline silicon on oxide contacts (POLO) [69–71], monofacial poly-Si contacts (monoPoly) [72, 73], or most frequently as tunnel oxide passivated contacts (TOPCon) [74–79]. The HIT and poly-Si architectures both feature carrier-selective, passivating contacts aimed at suppressing contact recombination. Other carrier-selective, passivating contact technologies exist and have their own advantages and disadvantages, but are not the focus of this review as they are still in the early stages of development. Additionally, interdigitated back contact (IBC) cells [80–82] are another cell structure that eliminates the use of metallization on the front side of the cell, thereby reducing the optical loss associated with light being reflected off these metal contacts. The IBC concept can be combined with other approaches, including heterojunctions and polysilicon-based passivating contacts to form very high efficiency cells, as in the current record holding 26.8% cell that is an IBC heterojunction [8, 9].

In this article we consider the major photon management schemes, from the more conventional approaches, like the use of antireflection coatings (ARC), to more novel and recently developed approaches for these various cell architectures. Section 2 explains the underlying physics and materials properties that dictate the various energy conversion losses in a cell. These are categorized as optical (i.e., photons lost), recombination (i.e., charge carriers lost through recombination), and resistive (e.g., voltage drop via inefficient charge transport). Section 3 provides an up-to-date review of the major photon management approaches in terms of optical benefits, as well as their impact on recombination and resistive losses when incorporated into cells. Section 4 presents a comprehensive and objective analysis of the optical performance of the various schemes using optical simulations of the reflectance and quantum efficiency curves. In Section 5, a critical examination of newly developed photon management structures that have not yet been implemented in practical photovoltaic cells is conducted. The merit of these structures is evaluated based on the findings of previous sections. Finally, Section 6 presents the overall conclusions.

2. Loss Mechanisms in Photovoltaic Cells

The efficiency of a PV cell depends on factors including its architecture, internal quantum efficiency, the quality of the active material (i.e., Si in our discussion), contact structure, photon management schemes, as well as any loss mechanisms present in the cell [56, 83, 84]. In studying how to effectively manage photons, it is crucial to recognize the various losses that can occur in PV cells, as the reflection loss, recombination loss, and resistive loss are all interconnected. A particular photon management approach may yield an optical gain, but if it also leads to increased recombination or resistive losses, that must be taken into account. Therefore, the optical design of a PV cell must prioritize increasing photocarrier generation while also minimizing recombination and resistive losses for practical applications.

Light trapping structures on both the front and rear sides of the cell are crucial for trapping incident photons within the active material and boosting photocurrent. The photogenerated current density J_G , which is ideally equal to the short-circuit current density of a cell J_{SC} is expressed by the following equation,

$$J_G = J_{SC} = e \int [1 - R(\lambda)] \Phi_{inc}(\lambda) IQE(\lambda) d\lambda \quad (1)$$

Here Φ_{inc} is the incident photon flux, IQE is the internal quantum efficiency and R is the percentage reflected light (i.e., loss). R is the summation of both front reflectance, R_f and the escape reflectance, R_{esc} (light that enters into the cell through front side, is not absorbed by Si, becomes reflected from the rear side, is not absorbed by Si again and then exits the cell through the front side). For a typical silicon PV cell R_{esc} becomes significant near the band edge. Light trapping structures on the front side reduces front reflectance, which in turn leads to an increase in J_{SC} . Similarly, if steps are

taken to reduce the escape reflectance on the rear side of the cell, this also promotes light absorption in the active region of the cell.

A good proportion of the incident photons are not captured by the cell due to shadowing caused by the front side metal contacts, such as busbars and gridlines, which are utilized for the efficient collection of photogenerated current. The proportion of contact area varies greatly depending on the type of cell and its contact structure. In industrial PV cells, the front contact area can range from 4% to 5% [85]. Additional optical losses can occur in the non-active regions of the cell, such as parasitic absorption in the emitter and antireflection coating layer, but these losses are relatively minor compared to the other types of optical losses previously mentioned [86].

Silicon is an indirect band-gap material, which makes a rapid drop in its absorption coefficient as the incident wavelength approaches the band gap energy (i.e., 1.1 eV or 1127 nm). This means that the thickness required to absorb all qualified photons (absorption length, L) increases rapidly with wavelength. For example, at 800 nm wavelength, $L \approx 10 \mu\text{m}$, while at 1100 nm wavelength, $L \approx 3 \text{ mm}$ [87]. A 6 mm thick silicon wafer can absorb all the light with energy above the band-gap, but it is not practical for carrier transport or cost. i.e., photogenerated electrons and holes now have to travel a greater distance before they can be extracted, and by doing so they lose their energy through nonradiative recombination process in the presence of crystalline imperfections in the bulk [88]. Rear side photon management improves absorption by providing additional chances for long wavelength photons to be absorbed, measured by path length enhancement. A path length enhancement factor of up to 10 can be achieved [89, 90]. Therefore, both front and rear side light trapping are necessary for efficient use of sunlight.

Recombination loss has a major impact on a cell's efficiency. Crystalline defects, dislocation centers, trap states in the Si wafer act as Shockley-Read-Hall recombination centers. Excessive doping of the emitter can also lead to Auger recombination. Some photon management schemes may improve optical performance but also increase surface recombination by exposing bare surface. Surface recombination loss can be reduced by passivating dangling bonds with another material or using a carrier selective contact structure [91]. A good PV cell should have both surface passivation and light trapping mechanisms.

The thickness of the wafer used in PV cell manufacturing is also important. A thinner wafer requires a strong photon management mechanism to ensure absorption. However, a thinner cell with well-passivated surfaces and high photogenerated current density may have a higher open circuit voltage (V_{oc}) due to lower dark saturation current density J_0 , as evident from equation (2) [92, 93].

$$V_{OC} = \frac{K_B T}{e} \left(\frac{J_{SC}}{J_0} + 1 \right) \quad (2)$$

Here K_B is the Boltzmann constant, T is the temperature and e is the charge of an electron. Thinner cells are harder to manufacture and have more difficulty with surface passivation, which can break during the process. Thicker wafers are easier to passivate and trap light but have more defects and trap states that increase J_0 , and also increase material costs. It's important to choose the right thickness while considering these trade-offs.

Now, the current density vs. voltage (J-V) characteristics of the cell is influenced by all the parameters discussed above.

$$J = J_{SC} - J_0 \left[\frac{V + J R_S}{n V_T} - 1 \right] \quad (3)$$

Here n is the diode ideality factor, R_S is the series resistance, and V_T is the thermal voltage. The efficiency of the cell, η can be expressed as,

$$\eta = \frac{V_{OC} * J_{SC} * FF}{P_{in}} \quad (4)$$

Here FF is the fill factor of the cell, which expresses the measure of how much rectangular is the J-V curve, a phenomenon that is greatly influenced by the recombination and resistive losses.

Designing and implementing an ideal photon management scheme is complex as it involves multiple factors and can only be considered useful when it improves the overall efficiency of the cell. In this article, we review contemporary photon management schemes and evaluate their performance based on the parameters discussed above.

3. Progress in Photon Management

The major challenges for achieving the Shockley–Queisser limit in crystalline silicon (c-Si) PV cells are incomplete light trapping and parasitic optical absorption [1]. Various photon management techniques have been studied to address these issues, including reducing losses, enhancing the optical path, and increasing the probability of photon absorption [2]. However, not all photon management techniques are suitable for all types of PV cells, such as aluminum-back surface field (Al-BSF), heterojunction (HIT) [64], interdigitated back contact (IBC) [82], passivated

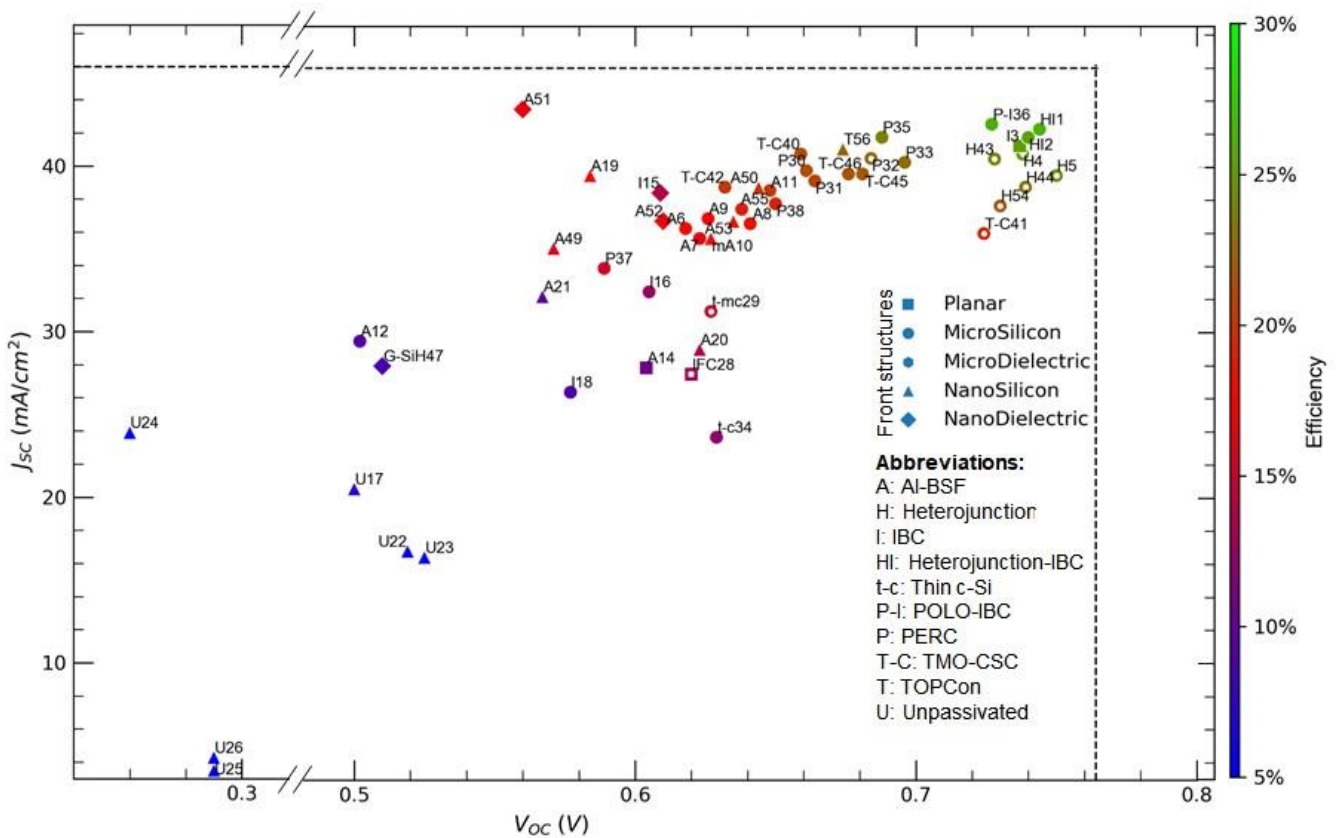


Figure 2: Impact of front side photon management structures and cell types on the short-circuit current density (J_{sc}), open-circuit voltage (V_{oc}), and efficiency of silicon photovoltaic cells. The horizontal and vertical dotted lines represent the highest achievable J_{sc} and V_{oc} values, respectively. Performance parameters for each cell are provided in Table 1, and the data point annotations in the figure correspond to the cell types and the serial numbers in that table.

emitter and rear contact (PERC) [59], IBC with polycrystalline silicon on oxide (POLO) contact [69], tunnel oxide passivated contact (TOPCon) [79] and unpassivated cells. The applicability of a particular photon management scheme depends on the contact structure and surface passivation of the cell type.

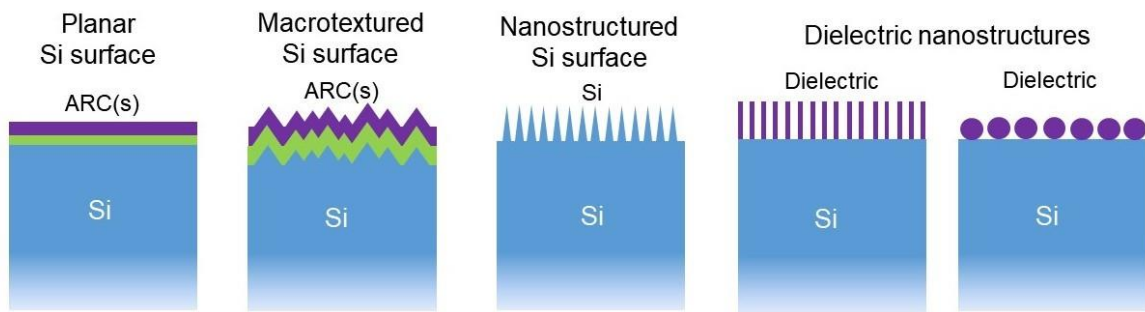
The performance of different types of PV cells are shown in Fig. 1, with overall efficiency (η) represented by the colorbar. The V_{oc} and J_{sc} of the cells are shown in x and y axis respectively, and their performance parameters are listed in Table 1. The shape of the data points in the figure represents the front side photon management structures, and a white circle inside some of the data point means that their rear side is structured (i.e., not planar). The label of the data points includes the cell type and their serial number (SN) on Table 1. The vertical and horizontal dotted lines represent the maximum V_{oc} and J_{sc} values attainable from a c-Si PV cell respectively. The following sections will discuss these data samples in detail, providing a summary and evaluation of the optical and electrical performance of these PV cells in relation to different photon management approaches.

3.1. Front Side Photon Management Approaches

Various methods have been utilized to improve the transparency of the photovoltaic cells on the front side, such as applying an antireflective coating (ARC), texturing the surface, and utilizing resonators. A graphical representation of these techniques is presented in Fig. 3(a).

Single layer dielectric antireflective coating (ARC) is a straightforward method to reduce reflection losses. Silicon Nitride (SiN_x) is commonly used as the coating material [95, 96] due to its lower refractive index (≈ 2) than

(a) Front structures



(b) Rear structures

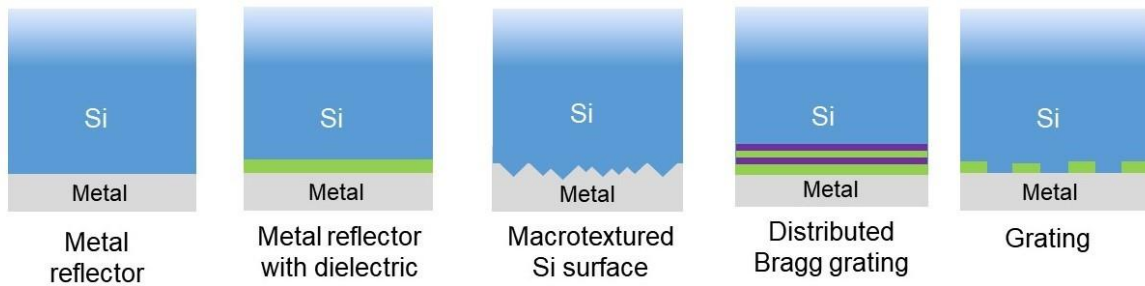


Figure 3: Schematic representation of different photon management structures employed on the front and rear sides of a silicon solar cell (reproduced from [94]).

crystalline silicon (≈ 4). Single layer ARC has the potential to achieve 100% optical transmission at the corresponding wavelength. Due to its simple fabrication process and low cost, dielectric ARC is widely used in commercial PV cells. However, it should be noted that the optical performance of single layer ARC is dependent on wavelength and polarization, and it has limited angular optical response which can be a drawback in practical applications [97].

To broaden the spectral and angular responses of ARC, various strategies have been examined. These methods can currently be divided into two categories: patterning on layers with different materials and direct patterning on the

silicon wafer (surface texturing). In these architectures, nano or microstructures with gradually varying geometries are positioned above the silicon wafer, resulting in higher transmission. Unlike traditional single layer ARC, these approaches exhibit an omnidirectional and broadband optical response due to the graded index distribution and thus destructive interference of a wide range of wavelengths, which is crucial for PV cells.

Antireflective nanostructures with different shapes have been studied, including nanowires, nanopillars, nanodomes, nanospheres, nanorods, and nanocones. For example, Jeong *et al.* investigated the performance of an ultra-thin silicon nanocone PV cell [98]. In this study, Si nanocones were fabricated on top of a Si substrate, and interdigitated Al contacts were placed on the rear side to prevent shadowing losses. It was reported that more than 80% external quantum efficiency (EQE) was demonstrated for 400-800 nm incident wavelengths. According to the current density-voltage relation, a V_{oc} of 0.623 V and J_{sc} of 29 mA/cm^2 were achieved, resulting in an efficiency of 13.7%. In addition to the antireflection effect, enhanced light scattering from these structures also contributed to the light trapping.

Nanowires are another effective geometry in light management. Lee *et al.* reported a radial junction PV cell with hybrid silicon wire structures [99]. In this configuration, p-n junctions were formed along the radius of silicon microwire arrays. The n-type microwires were deposited on a thick Czochralski silicon (Cz-Si) wafer while p-type nanowires were deposited on top of them. This design shortened the traveling path of the charge carriers, thus reducing recombination losses. The combined effects of graded index structures and light trapping between the wires significantly reduced reflection losses, resulting in 97% absorption of total incident light. In this configuration, a V_{oc} of 0.584 V and J_{sc} of 39.5 mA/cm^2 were achieved, resulting in an efficiency of 17.6%.

Surface texturing is another method of enhancing the optical performance by increasing transmission and reducing reflection losses. The main difference between surface texturing and antireflective nanostructure is that surface texturing is directly etched or deposited on the substrate, without adding a new layer with different materials. Therefore, surface texturing has a simple fabrication process. Similar to antireflective nanostructures, enhanced transmission into the cell is achieved through altered internal angles and graded refractive index caused by gradually varying geometry. For example, Kafle *et al.* [100] reported a nanotextured multicrystalline (mc-Si) PV cell in which nanotextures were etched on a 195 μm thick p-type mc-Si wafer by dry exothermic plasma etching. An Al-BSF layer formed through screen printing Al paste and annealing was placed on the rear side of the cell as a metallic back contact. The structure achieved 0.627 V V_{oc} and 36.7 mA/cm^2 J_{sc} simultaneously, resulting in 18% efficiency. Fellmeth *et al.* reported another Al-BSF c-Si PV cell with pyramid texturing on the front surface [101]. In this study, 0.648 V V_{oc} and 38.6 mA/cm^2 J_{sc} are reported, resulting in an overall efficiency of 20.1%. A cost-effective form of nanostructured silicon is called black silicon (b-Si) due to its low reflection, which is another candidate for light trapping. B-Si has a wide absorption spectrum, especially in the visible and infrared range, resulting in high efficiency. Savin *et al.* reported a b-Si PV cell with interdigitated back contacts (IBC) that mitigated reflection losses on the front side [102]. The b-Si was fabricated by deep reactive ion etching (DRIE). Due to the needle-like silicon textures with high aspect ratio, an effective medium was formed. As a result, most of the reflection loss was eliminated. In this cell, 0.665 V V_{oc} and 42.2 mA/cm^2 J_{sc} were achieved, leading to 22.1% efficiency.

An alternative approach of improving the device performance is incorporating optical resonators. When nanoparticles are embedded inside the PV cell, the field distribution is highly confined in the active layer by the excited resonant modes, thus enhancing the absorption of the incident photons. However, additional plasmonic absorptions can be induced by metallic nanoparticles. Various materials have been adopted as nano resonators, including dielectric (Mie resonance) and metallic (plasmon resonance) materials. By applying particles with different sizes, multiple resonant

peaks are excited, resulting in broadband optical response. Additionally, these nanoparticles also scatter light, extending the length of the optical path inside the active region. For instance, Yao *et al.* [103] reported a broadband spherical nanoshell PV cell. In this configuration, a single layer of silicon nanospheres with 50 nm thickness was deposited on a 1 μm silicon substrate. The incident light was coupled into whispering-gallery modes (WGMs) inside the spheres and transmitted into the substrate. Multiple resonant modes with different resonant peaks were excited, leading to broadband optical absorption. In this arrangement, 0.51 V V_{oc} and 20.1 $\text{mA}/\text{cm}^2 J_{sc}$ were demonstrated, resulting in 8.1% efficiency. It is important to note that this result was based on the theoretical simulation of a p-i-n PV cell without additional efficiency enhancement approaches, and the generation of photoelectrons were approximated, leading to a relatively low efficiency.

3.2. Rear Side techniques

The incident light may exit the PV cell when it is not fully absorbed in the active region and minority carriers may suffer from surface recombination on the rear side of the cell, both of which limit the efficiency of the cell. To improve the performance of the cell, optimizations on the rear side are required. Similar to the front side, both optical and electrical approaches have been employed, including full and partial covering, such as aluminum back

Table 1: Cell Performance Parameters

SN	Front Structure	Rear Structure	Thickness of Si (μm)	Cell Type	V_{oc} (V)	J_{sc} (mA/cm^2)	FF (%)	Efficiency (%)	Reference
1	MicroSi	Planar	165	Heterojunction-IBC	0.744	42.3	83.57	26.3	[104]
2	MicroSi	Planar	150	Heterojunction-IBC	0.74	41.8	82.76	25.6	[105]
3	Planar	Planar	130	IBC	0.737	41.3	82.79	25.2	[106]
4	MicroSi	MicroSi	160	Heterojunction	0.738	40.8	83.36	25.1	[107]
5	MicroSi	MicroSi	98	Heterojunction	0.75	39.5	83.37	24.7	[108]
6	MicroSi	Planar	180	Al-BSF	0.618	36.3	79.34	17.8	[96]
7	MicroSi	Planar	150	Al-BSF	0.623	35.7	75.53	16.8	[95]
8	MicroSi	Planar	150	Al-BSF	0.641	36.6	77.58	18.2	[95]
9	MicroSi	Planar	150	Al-BSF	0.626	36.9	75.76	17.5	[95]
10	NanoSi	Planar	195	mAl-BSF	0.627	35.7	80.41	18	[100]
11	MicroSi	Planar	225	Al-BSF	0.648	38.6	80.36	20.1	[101]
12	MicroSi	Planar	75	Al-BSF	0.502	29.5	62.39	9.24	[109]
13	Planar	NanoDi	0.450	Thin-aSi	0.83	14.07	56.08	6.55	[110]
14	Planar	Planar	280	Al-BSF	0.604	27.9	62.31	10.5	[111]
15	NanoDi	Planar	-	IBC	0.609	38.45	59.96	14.04	[112]
16	MicroSi	Planar	-	IBC	0.605	32.48	65.19	12.81	[112]
17	NanoSi	Planar	10	Unpassivated	0.5	20.59	69.84	7.19	[113]
18	MicroSi	Planar	-	IBC	0.577	26.42	58.84	8.97	[112]
19	NanoSi	Planar	200	Al-BSF	0.584	39.5	76.29	17.6	[99]
20	NanoSi	Planar	10	Al-BSF	0.623	29	75.83	13.7	[98]

21	NanoSi	Planar	-	Al-BSF	0.567	32.2	52.09	9.51	[114]
22	NanoSi	Planar	20	Unpassivated	0.519	16.82	60.71	5.3	[115]
23	NanoSi	Planar	8	Unpassivated	0.525	16.45	55.93	4.83	[115]
24	Planar	Planar	-	Unpassivated	0.26	23.9	54.71	3.4	[116]
25	Planar	Planar	0.225	Unpassivated	0.29	3.5	49.26	0.5	[117]
26	Planar	Planar	-	Unpassivated	0.29	4.28	37.06	0.46	[118]
27	NanoSi	NanoSi	0.280	Thin-aSi	0.75	17.5	44.95	5.9	[119]
28	Planar	MicroSi	675	IFC	0.62	27.5	77.42	13.2	[87]
29	MicroSi	NanoSi	20	Thin-mcSi	0.627	31.3	77.45	15.2	[120]
30	MicroSi	Planar	-	PERC	0.661	39.8	80.58	21.2	[121]
31	MicroSi	Planar	-	PERC	0.664	39.18	79.95	20.8	[122]
32	MicroSi	MicroSi	-	PERC	0.684	40.54	81.54	22.61	[123]
33	MicroSi	Planar	-	PERC	0.696	40.3	81.28	22.8	[57]
34	MicroSi	Planar	-	TMO-CSC	0.629	23.7	82.51	12.3	[124]
35	MicroSi	Planar	180	PERC	0.687 9	41.81	82.85	23.83	[125]
36	MicroSi	Planar	290	PERC	0.727	42.6	84.27	26.1	[126]
37	MicroSi	Planar	10	PERC	0.589	33.9	78.63	15.7	[127]
38	MicroSi	Planar	43	PERC	0.65	37.8	77.74	19.1	[128]
39	MicroSi	Planar	180	TMO-CSC	0.659	40.8	79.22	21.3	[129]
40	MicroSi	MicroSi	200	TMO-CSC	0.724 2	36	74.03	19.3	[130]
SN	Front Structure	Rear Structure	Thickness of Si (μm)	Cell Type	V_{oc} (V)	J_{sc} (mA/cm^2)	FF (%)	Efficiency (%)	Reference
41	MicroSi	Planar	200	TMO-CSC	0.632	38.8	81.97	20.1	[131]
42	MicroSi	MicroSi	230	Heterojunction	0.728	40.5	81.09	23.91	[132]
43	MicroSi	MicroSi	150	Heterojunction	0.739	38.8	80.60	23.11	[132]
44	MicroSi	Planar	155	TMO-CSC	0.681	39.6	80.84	21.8	[133]
45	MicroSi	Planar	175	TMO-CSC	0.676	39.6	80.69	21.6	[134]
46	NanoDi	Planar	20	Gr-Si Heterojunction	0.51	28	61.62	8.8	[135]
47	NanoDi	Planar	> 0.032	Thin-aSi	0.885	9.24	60.90	4.98	[136]
48	NanoDi	Planar	50	Al-BSF	0.571	35.11	79.21	15.88	[137]
49	NanoSi	Planar	-	Al-BSF	0.644	38.77	79.30	19.8	[138]
50	NanoDi	Planar	-	Al-BSF	0.56	43.5	68.14	16.6	[139]
51	NanoDi	Planar	-	Al-BSF	0.61	36.75	74.90	16.79	[140]
52	NanoSi	Planar	200	Al-BSF	0.635	36.74	79.81	18.62	[141]
53	MicroSi	MicroSi	200	Heterojunction	0.73	37.67	79.42	21.84	[142]

54	MicroSi	Planar	200	Al-BSF	0.638	37.47	78.93	18.87	[143]
55	NanoSi	Planar	-	TOPCon	0.674	41.1	80.50	22.3	[144]
56	NanoSi	Planar	170	TOPCon	0.696	41.44	81.69	23.55	[145]
57	MicroSi	MicroSi	-	TOPCon	0.717	40.57	84.52	24.58	[146]

Elaboration: MicroSi=microscale silicon, NanoSi=nanoscale silicon, NanoDi=nanoscale dielectric.

surface field (Al-BSF) and passivated emitter and rear cell (PERC), which act as a rear side passivation layer that keeps the minority carriers away from the highly recombining rear surface, and interdigitated back contacts (IBC) cell that place the metal contacts on the rear side of the cell to avoid shading losses on the front side. Additionally, resonators and grating structures have been reported in some configurations to boost the overall performance by exciting resonant modes. In practice, combined techniques are employed to further improve the efficiency.

In Al-BSF PV cells, an Al back reflector is printed on the rear side of the silicon wafer to recover any transmitted light. By increasing the optical path of the incident photons, the chances of absorption in the active region are increased. Additionally, a passivation layer doped with phosphorus is added on the front side of the cell, decreasing the resistance at the metal-silicon interfaces and reducing the impact of surface defects and recombination losses.

A p-type Al-BSF silicon PV cell was reported by Vermang *et al.* [95] in which the performance of various types of Al-BSF PV cells with blistered (bubble-like) rear surface passivation were compared. It was reported that Al-BSF PV cells achieved a high V_{oc} of 0.627 V, $36.9 \text{ mA/cm}^2 J_{sc}$ and 17.4% efficiency. Full Al-BSF cells achieved 0.623 V V_{oc} , $35.7 \text{ mA/cm}^2 J_{sc}$ and 16.8% efficiency. It was demonstrated that local Al-BSF PV cells exhibited the best performance among other types, with 0.641 V V_{oc} , $38.7 \text{ mA/cm}^2 J_{sc}$ and 18.2% efficiency reported. It was shown that local Al-BSF cells provide good performance due to enhanced reflection on the rear side and improved surface passivation.

In passivated emitter and rear cell (PERC), the shading losses are significantly reduced by relocating the contacts onto the rear side of the cell. Localized passivation contacts are added on the rear side to reduce the recombination loss and increase back-reflection. Unlike Al-BSF PV cells, localized back surface fields are printed above the rear contacts as back reflectors to enhance the absorption of the incident photons. For example, Hannebauer *et al.* reported a fine-line printed PERC PV cell [147]. In this study, a commercial PERC cell with 5 busbar front grids and fineline-printed Ag fingers were evaluated. It was reported that shading losses were reduced to 4% compared to 5.8% of conventional 3 busbar structures. It was reported that high V_{oc} of 0.661 V and J_{sc} of 39.8 mA/cm^2 were achieved, resulting in 21.2% efficiency. Huang *et al.* reported a PERC cell with ALD aluminum rear surface passivation [122]. A $190 \mu\text{m}$ thick p-type Cz-Si wafer is used as the substrate. Excellent performance of 0.664 V V_{oc} and $39.18 \text{ mA/cm}^2 J_{sc}$ was reported, resulting in an overall efficiency of 20.8%. Additionally, Deng *et al.* reported a fully screen-printed PERC cell with high efficiency [123]. In this study, the silicon wafer had a thickness of $175 \mu\text{m}$. The increased efficiency was mainly due to the reduced resistivity of the contacts and front finger lines. It was reported that 0.684 V V_{oc} and $40.48 \text{ mA/cm}^2 J_{sc}$ were achieved, resulting in a high efficiency of 22.61%.

In interdigitated back contact (IBC) PV cells, the metallic contacts are placed on the rear side of the cells in order to eliminate shading losses on the front side. These contacts also act as back reflectors. Both sides of the silicon wafer are etched with surface textures, leading to longer optical path that increases the absorption of photons in the active region. Additionally, a thin layer of the same material (a-Si) is placed between the silicon wafer and a doped a-Si layer to passivate the interface on the rear side of the cell, which improves the total quantum efficiency. For example, Smith *et*

al. have reported an IBC PV cell with total area efficiency above 25% [106]. Contact pads and busbars were placed on the bottom of a 130 μm thick c-Si wafer. As a commercial product, both high optical and electrical performances were reported. It was demonstrated that 0.737V V_{oc} and 41.3 mA/cm^2 J_{sc} were achieved by the cell, resulting in an overall 25.2% efficiency. Improvements in recombination losses on the edge and series resistances were also reported in comparison to previous products. Yoshikawa *et al.* reported a heterojunction interdigitated back contacts (HJ-IBC) silicon PV cell with pyramid texturing [104]. In their study, microscale textured pyramid structures were fabricated on a 165 μm thick silicon substrate by anisotropic etching. The cell achieved 0.744 V V_{oc} and 42.3 mA/cm^2 J_{sc} , resulting in an extraordinary efficiency of 26.3%. Another configuration incorporating polo-IBC PV cell was reported by Hollemann *et al.* [38]. In this study, passivating polo-IBC (poly-silicon of oxide junctions) contacts are placed in the rear side of the silicon PV cells, as shown in figure 8(a). Efficiency of 26.1% and 24.9% on p-type FZ wafers with resistivity of 1.3 $\Omega\text{-cm}$ and 80 $\Omega\text{-cm}$, and 24.6% on a n-type wafer with 2 $\Omega\text{-cm}$ resistivity were obtained. The 26.1% efficient cell exhibited a J_{sc} of 42.6 mA/cm^2 and a V_{oc} of 0.727 V. Infrared lifetime mapping showed potential for further improvement by reducing losses from series resistance, perimeter recombination, process-induced degradation, and bulk recombination.

Nanostructures, such as nanocones, are also used for light trapping on the rear side. For example, in a study by Zhu *et al.*, a-Si:H PV cells with nanocone back reflectors were reported [119]. In this study, a-Si nanocones in the scale of hundreds of nanometers were deposited on the substrate with the same material, forming periodic nanodome structures under a p-i-n a-Si layer sandwiched between transparent conducting oxides (TCO) layers. The tapered shape of the nanodomains generated excellent antireflection properties, and the matching of the a-Si index with air greatly reduced front-side reflection loss. Additionally, incident light scattering was enhanced inside the plane, resulting in an enhanced optical path and improved absorption. This design yielded a V_{oc} of 0.75 V and J_{sc} of 17.5 mA/cm^2 , resulting in an efficiency of 5.9%.

Grating structures on the rear side of a cell have been studied for their ability to support resonant modes and scatter light for improved optical path length. Zeng *et al.* [87] reported a hybrid grating-photonic crystal back reflector silicon PV cell. The design included a reflection grating on the rear side of the cell and a 1D distributed back reflector (DBR) layer beneath the grating. The cell thickness was 675 μm , with metallic contact on the front side. The DBR achieved over 99.8% reflectance in the wavelength range of 800-1100 nm. This design resulted in a V_{oc} of 0.62 V and J_{sc} of 27.5 mA/cm^2 , yielding an efficiency of 13.2%.

Resonant modes also improve light harvesting on the rear side of a PV cell. Tu *et al.* reported using double wall carbon nanotubes (DWCNTs) in amorphous silicon (a-Si) PV cells [110]. The DWCNTs were spin-coated on Ti/Ag back contacts to excite plasmon resonances and enhance light scattering in the range of 589-700 nm. By adjusting the ratio of DWCNTs to polymers, the resonance region was adapted to the desired wavelength range. The reported V_{oc} and J_{sc} were 0.83 V, and 14.07 mA/cm^2 respectively, yielding an efficiency of 6.55%

3.3. Comprehensive Analysis of Front and Rear Side Photon Management Techniques

Fig. 2 displays performance parameters of various recently made Si PV cells, including their corresponding photon management techniques, and cell type. The maximum attainable V_{oc} and J_{sc} from a c-Si PV cells are shown as dotted lines. Table 1 provides additional information on these cells.

The importance of surface passivation is evident in the unpassivated PV cells represented by the data points U17, U22, and U23, which have nanosilicon structures on the front side and planar rear side. Poor passivation of the front nanostructures resulted in recombination loss and reduced efficiency. U24, U25, and U26 are Si nanowire-based PV cells

with no notable photon management structures. These cells have low voltage, likely due to the reduced bandgap energy of the Si nanowires, resulting in more band-to-band transitions for U24, resulting in higher J_{sc} . However, unpassivated surfaces caused some loss and reduced final J_{sc} . The other two nanowire cells probably had higher series resistance in addition to high surface recombination, resulting in even lower efficiency.

Many data points represent Al-BSF cells, a type of cell that has dominated the industrial PV market for a long time. In the rear side of these cells, the BSF layer formed through Al screen printing and annealing acts as both a passivation layer and reflector. A variety of structures are employed on the front side, including planar, microsilicon, nanosilicon, and nanodielectric structures for photon management. The highest efficiency Al-BSF cell (A11, 20.1% efficiency) has a microsilicon front structure, providing J_{sc} of 38.6 mA/cm^2 with a Si thickness of $225 \mu\text{m}$. The next highest efficiency Al-BSF cell (A49, 19.8% efficiency) has a J_{sc} of 38.77 mA/cm^2 . It is important to note that front-side nanostructures have slightly higher J_{sc} values but slightly lower V_{oc} and FF values in the case of A49, likely due to poor surface passivation of the nanostructures. The lowest efficiency Al-BSF cell (A12, 9.24% efficiency) has a microsilicon front structure, poor performance in terms of V_{oc} , J_{sc} , and FF , indicating high recombination. Additionally, the thickness of $75 \mu\text{m}$ was not sufficient for capturing incident photons, contributing to the lower J_{sc} .

PERC cells are currently the dominant PV cells in the global market [148, 149]. These cells have passivated front and rear sides, reducing surface recombination and achieving high V_{oc} , J_{sc} and FF values with the same photon management as Al-BSF cells. For instance, P47 achieved 21.2% efficiency with a V_{oc} of 0.627 V, J_{sc} of 39.8 mA/cm^2 and FF of 80.58% using a microsilicon front and planar rear. Structuring the rear side while maintaining good surface passivation improves performance further, as seen in cell P32, which has microsilicon structures on both sides and achieved a V_{oc} of 0.684 V, J_{sc} of 39.8 mA/cm^2 , FF of 81.54%, and efficiency of 22.61%

The TOPcon cell [150] is a new type of PV cell that significantly reduces surface recombination by utilizing a thin tunneling oxide to passivate the contact, keeping the contact resistivity of the cell almost unchanged. In one of these cells (T55), nanosilicon front side and planar rear provided 41.1 mA/cm^2 J_{sc} , pointing to a good photon management arrangement. This cell achieved a V_{oc} of 0.674 V and an efficiency of 22.3%. However, it was found that the surface passivation of the nanosilicon structure in T55 was not sufficient, prompting the introduction of a new nanosilicon structure in T56 that reduces the difficulty of passivation. This new structure, which involves forming a random pyramid texture and then creating nanoscale pores through reactive ion etching, resulted in increased photocurrent density, V_{oc} and efficiency compared to T55. Another TOPcon cell, T57, used a microsilicon structure on both sides, but did not achieve as high photocurrent density as T55 and T56 due to its relatively higher front reflectance. However, the passivation quality of the microsilicon structure was better, resulting in a higher V_{oc} and efficiency. These examples demonstrate that increasing the photogenerated current does not always improve cell performance and a comprehensive analysis should be conducted when implementing a photon management approach.

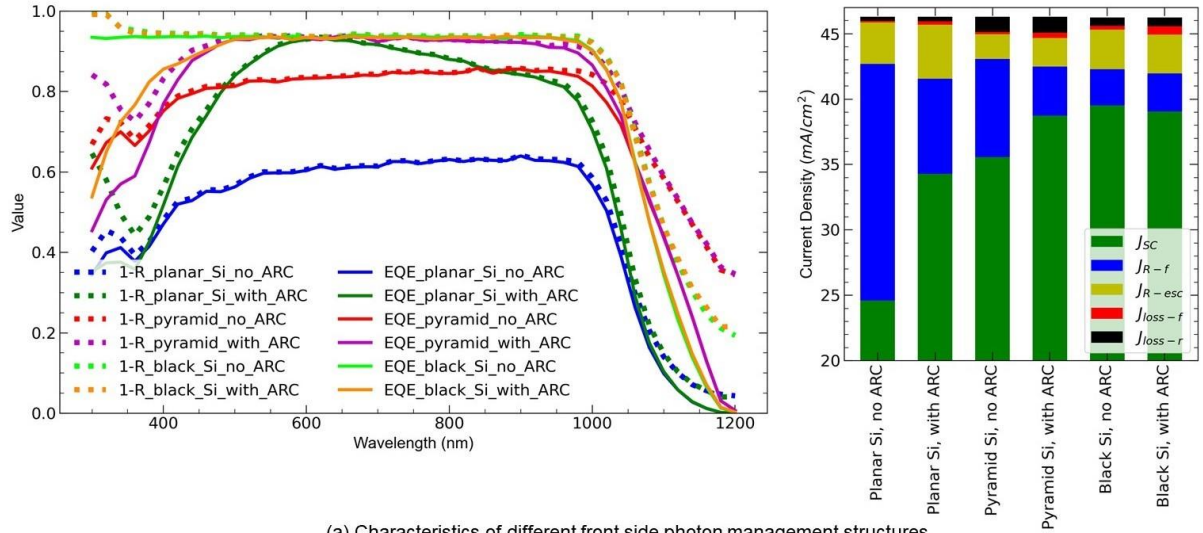
The heterojunction cells in the dataset have achieved relatively higher efficiency by using microsilicon structures on both the front and rear sides. This high performance was achieved due to effective photon management, selecting the appropriate cell thickness, and proper surface passivation. For example, H4 demonstrated a V_{oc} of 0.738 V, a photocurrent density of 40.8 mA/cm^2 , and a FF of 83.36%, resulting in an efficiency of 25.1%. Its performance was surpassed by H2, which achieved an efficiency of 25.6% by using a heterojunction-IBC structure. H2 had a V_{oc} and FF that were similar to H4, but the main improvement came from an increase in photocurrent density (41.8 mA/cm^2) due to the adoption of an IBC structure on the rear side which also trapped some light to the cell.

While it is common to have a textured front and a planar rear side in solar cells, there are also cases where the opposite is used. For instance, the cell IFC28 has a planar front side and a photonic crystal back reflector with a grating structure on the rear side. This arrangement resulted in a photocurrent density of 27.5 mA/cm^2 . The V_{oc} and FF of this cell were 0.62 V and 77.42% , respectively. However, the photocurrent density could have been further improved if the front side also had a photon management scheme. Additionally, the cell thickness of $675 \mu\text{m}$ is much greater than the diffusion length [151, 152] of silicon, which is between $100\text{-}300 \mu\text{m}$ [86, 153, 154]. This resulted in nonradiative recombinations and could have led to even better V_{oc} , photocurrent density and fill factor.

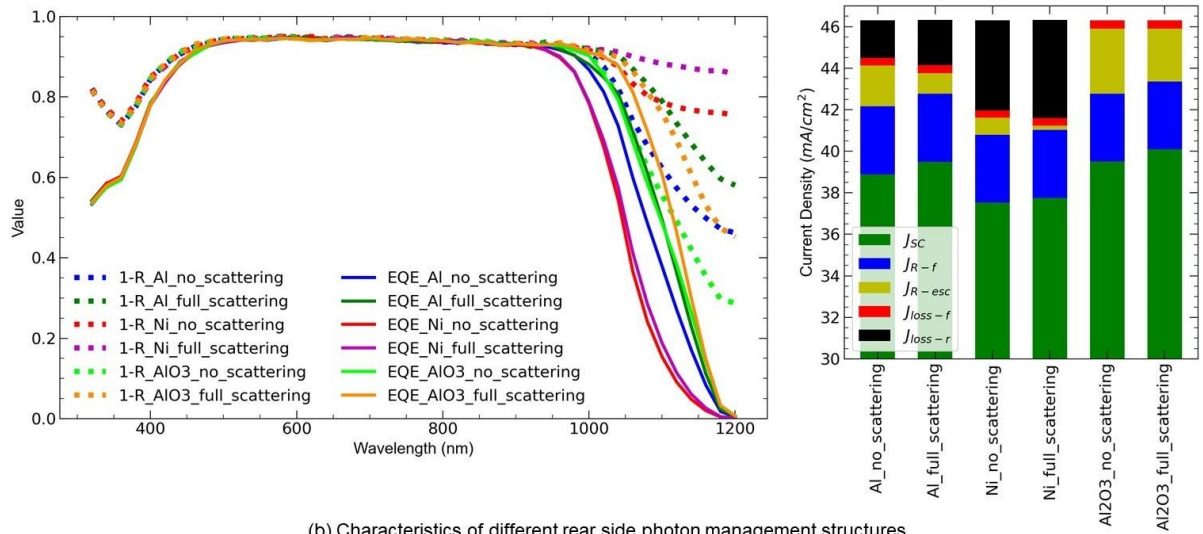
A number of cells were investigated with nanodielectric structures on the front side, which provided some level of light trapping compared to cells with no structure on the front. However, these schemes failed to achieve significant efficiency. For example, GSiH46 achieved a V_{oc} of 0.51 V , a photocurrent density of 28 mA/cm^2 , and a FF of 61.62% using a bilayer graphene on the front side and a planar rear side. The front reflectance of the cell was less than 5% for the wavelength range of $520\text{-}700 \text{ nm}$ and less than 10% for longer wavelengths, indicating that the cell was able to capture a good number of photons, yet failed to achieve high efficiency. There are several reasons for this. Firstly, it used whispering gallery mode [155, 156] to confine incident light to the cell. However, in this arrangement, perpendicularly incident light does not see any redirection by the front side, as is usually seen for pyramid textured front surfaces (microsilicon structure) [91, 157, 158]. Secondly, the cell thickness of only $20 \mu\text{m}$ was not sufficient for adequate light trapping. Additionally, the lower values of V_{oc} and FF also indicate that the surface passivation quality was poor.

4. Practical Limit of Photon Management and Improvement Pathways

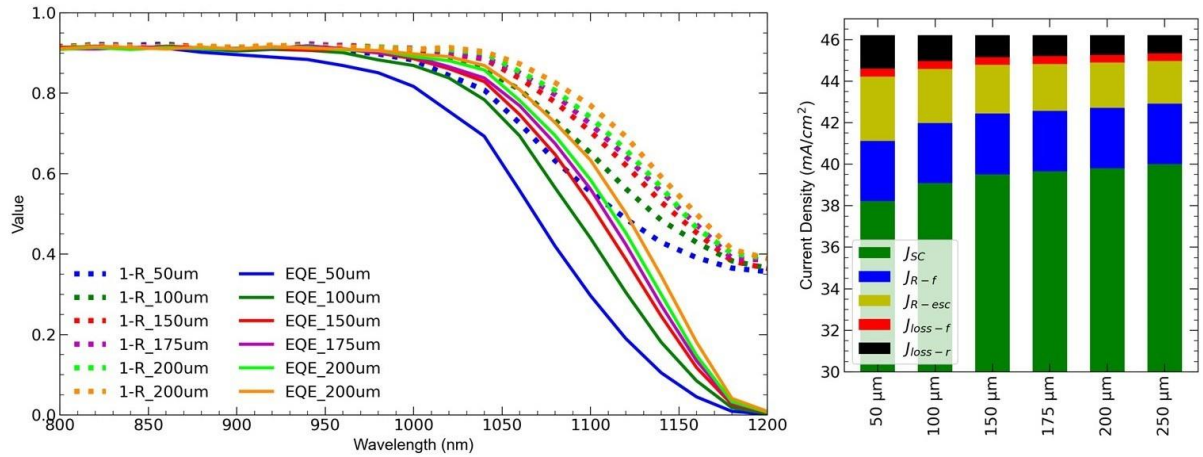
When searching for the most effective photon management approach, it is important to quantify the contribution of each technique. From our discussions, it has been found that microsilicon and nanosilicon structures have shown the greatest potential for use as front side photon management structures. Furthermore, when rear side structures such as microsilicon are used, they scatter incident light at an angle which enhances path length further. To determine the highest achievable photocurrent density practically in these configurations, a study was conducted using a simulation tool called SunSolve [159]. Pyramid structures were used as a representative of microsilicon structures and black silicon was used as a representative of nanosilicon structures for the front side. On the rear side, both metallic and



(a) Characteristics of different front side photon management structures (fixed rear side: PERC - 1 μ m AlSi+10nm Al₂O₃+100 nm SiN_x, no scattering. Wafer thickness: 175 μ m)



(b) Characteristics of different rear side photon management structures (fixed front side: 75nm SiN_x + pyramid texture. Wafer thickness: 175 μ m)



(c) Impact of cell thickness on photon management (Front: 5 μ m high random pyramid, 87.5° (black Si), no ARC Rear: PERC - 1 μ m AlSi contact + 10 nm Al₂O₃+ 100 nm SiN_x, full scattering)

Figure 4: Factors influencing photon management in a silicon solar cell. Legend: J_{sc} : short-circuit current density, J_{R-f} : loss in current density due to front reflectance, J_{R-esc} : loss in current density due to escape reflectance, J_{loss-f} : loss in current density (absorption) at the front side, and J_{loss-r} : loss in current density (absorption) at the rear side.

dielectric rear sides with and without full scattering characteristics were considered. Additionally, the impact of cell thickness in the presence of front and rear side photon management mechanisms was also studied.

The study presented in Fig. 4(a) investigates the performance of different front side photon management structures using a fixed rear side consisting of $1\ \mu\text{m AlSi} + 10\ \text{nm Al}_2\text{O}_3 + 100\ \text{nm SiN}_x$, with no scattering. The cell thickness for this study was $175\ \mu\text{m}$. The study considers three different front structures: a planar surface, a random pyramid texture, and black Si ($5\ \mu\text{m}$ tall, 87.5° sidewall angle), both with and without $75\ \text{nm SiN}_x$ on them. The first part of Fig. 4(a) shows the cell's 1-R (total absorption) and EQE (external quantum efficiency) over the solar spectrum, where R is the total reflectance of the cell. It is important to note that 1-R accounts for both the absorption in the active region of the cell and the parasitic absorption loss in the front and rear side of the cell [56, 83]. We observed that a PV cell with a planar silicon surface and no ARC on the front side was able to absorb approximately 60% of incident light in the 600-1000 nm wavelength range, with a decrease in absorption for other wavelengths. Analysis revealed a slight discrepancy between the EQE and 1-R in the shorter ($<400\ \text{nm}$) and longer ($>1100\ \text{nm}$) wavelength ranges, which was attributed to parasitic optical absorption on the front and rear sides of the cell, respectively. The addition of a $75\ \text{nm SiN}_x$ ARC on the planar front side significantly improved the 1-R and

EQE of the cell. Additionally, incorporating pyramid textures on the front side also greatly improved the 1-R and EQE compared to a planar surface without an ARC, but exhibited a lower performance in the 430-820 nm range. The highest EQE and 1-R values were achieved using a black silicon front, which was able to absorb approximately 95% of incident light. Notably, applying an ARC to the black silicon surface resulted in a slight decrease in EQE in the shorter wavelength range, due to parasitic absorption within the ARC. The bar chart in Fig. 4(a) breaks down the total incident light energy into various components including photogenerated current density (J_{sc}), loss in current density due to front reflectance (J_{R-f}) and escape reflectance (J_{R-esc}), and loss in current density due to parasitic optical loss on both the front (J_{loss-f}) and rear sides (J_{loss-r}) of the cell. Our findings indicate that the use of an ARC on planar silicon increased current density by $9\ \text{mA}/\text{cm}^2$, primarily as a result of reduced front reflectance loss, however it also slightly increased the escape reflectance loss. This is due to the Si-SiN_x-air boundary having a lower refractive index contrast than the Si-air boundary, making it easier for light to escape. Using a pyramid silicon surface with an ARC structure further reduced both front and escape reflectance loss. However, using a black silicon structure decreased front reflectance loss and parasitic optical loss on both the front and rear sides of the cell, but increased escape reflectance loss. To further reduce escape reflectance loss, the thickness of the cell could be increased until it reaches the minority carrier diffusion length of silicon, allowing for absorption of longer wavelength photons.

We examined the characteristics of various rear-side photon management structures, all of which had the same front structure consisting of a $75\ \text{nm SiN}_x$ ARC on a pyramid texture, with a wafer thickness of $175\ \mu\text{m}$. The structures evaluated included planar aluminum, aluminum structures designed to scatter light, planar nickel (a lossy metal with good electrical transport properties), nickel structures designed to scatter light, planar Al_2O_3 (which has poor electrical transport properties but excellent surface passivation), and Al_2O_3 structures designed to scatter light. Our findings, shown in Fig. 4(b), indicate that all of the rear structures displayed similar EQE and reflectance characteristics in the shorter wavelength range, which can be attributed to their consistent front side structure. However, the rear structure primarily influenced the absorption of longer wavelength photons. We observed that scattering structures generally exhibited higher absorption than their planar counterparts, as more of the unabsorbed light is reflected back and forth between the front and rear sides, increasing the total path length for silicon absorption. Additionally, we found that the highest absorption in the longer wavelength range was achieved with the nickel structure designed to scatter light,

followed by the planar nickel. However, these structures also exhibited the lowest EQE, indicating that most of the absorption occurred in nickel, rather than silicon, resulting in parasitic optical loss. The highest EQE in the longer wavelength range was observed in the case of the Al_2O_3 structure designed to scatter light, due to the absence of parasitic optical loss on the rear side, which is typically present in metals [149, 160–162]. The bar chart presented in Figure 4(b) supports the findings that Al_2O_3 structures did not exhibit any $J_{\text{loss-r}}$, while Ni structures exhibited the highest $J_{\text{loss-r}}$. Two key conclusions can be drawn from this information. Firstly, the J_{sc} achieved using the scattering Al_2O_3 structure was 40 mA/cm^2 . In order to increase the J_{sc} further with the same front structure, the cell thickness must be increased until it reaches the minority carrier diffusion length. However, exceeding this limit will result in recombination loss in the bulk. Secondly, it is important to note that Al_2O_3 is a dielectric material, using which on the entire surface prevents the collection of photogenerated carriers. Therefore, in practical applications, contacts must be created by covering a portion of the rear side with metal, which will result in parasitic optical loss in the metal and recombination loss at the Si-metal boundary, ultimately reducing the J_{sc} .

The impact of the cell thickness on the cell optical performance is illustrated in Fig. 4(c). The cell front side is assumed to be black Si without an ARC and the rear side is assumed to be composed of $1 \mu\text{m}$ AlSi, 10 nm Al_2O_3 , and 100 nm SiN_x with full scattering. As shorter wavelength photons are absorbed in the front side and are not affected by cell thickness, the 1-R and EQE characteristics in the wavelength range of $800 - 1200 \text{ nm}$ are presented. It can be observed that an increase in thickness led to an increase in 1-R and EQE, but the rate of increase slowed down with increasing thickness.

In light of the findings discussed above, the dataset presented in this paper (Table 1) was analyzed in more detail. The highest efficiency cell had an efficiency of 26.3%, which was achieved using a microsilicon front, planar rear, and $165 \mu\text{m}$ thickness. To enhance its light trapping further, a nanostructured front and micro-structured rear with scattering capabilities could potentially be used. However, passivating a nanostructured surface is a significant challenge. There have been recent advancements in passivating black Si [163–167] which could be utilized.

5. Photon Management Structures Not Yet Incorporated in Practical PV cells

Recent literature presents various photon management structures grown on isolated substrates or simulated, such as Heidarzadeh *et al.*'s idea for increasing photogenerated current in thin-film PV cells [168] using hemispherical coreshell nanoparticles on the front and triangular grating reflectors on the rear which achieved J_{sc} of 22 mA/cm^2 . The forward scattering of the core-shell nanoparticles is a positive aspect for J_{sc} but they incur plasmonic absorption, causing dips in the active material's absorption spectra and not fully utilizing the incident sunlight. Comparing this to our SunSolve simulation of planar Si and no ARC (1-R characteristics in Fig. 4(a)), it showed better absorption in Si for some wavelengths but poorer in others. However, it under-performs compared to our planar Si and ARC simulation. Therefore, using these core-shell nanoparticles does not significantly improve cell performance.

In a similar design, trapezoidal pyramid nanostructure (i.e., nanosilicon) are proposed for the front side and inverted pyramid nanotexture (i.e., nanosilicon) for the rear side of a $0.9 \mu\text{m}$ thick c-Si/ZnO heterojunction PV cell [169]. The simulations resulted in a J_{sc} of 41.94 mA/cm^2 , with a front reflectance of $\leq 5\%$ for $400 - 1000 \text{ nm}$ wavelength and higher for other wavelengths. Although the results are promising, it would be difficult to implement the nano-trapezoidal Si texture on the front side and passivate both sides, particularly the rear side where Si inverted pyramids are filled with Al.

Recently, Wang *et al.* has developed a ZnO nano-needle array (i.e., nanodielectric structure) for front-side photon management [170] on a textured Si substrate, which has been experimentally shown to reduce front reflectance to $\leq 8\%$ at 400-1000 nm wavelength. This structure achieved a J_{sc} of 37.8 mA/cm^2 , an increase of 1.8 mA/cm^2 compared to textured Si front surface. The advantage of this structure is that it avoids the challenge of passivating a nanostructured Si while providing similar front reflectance. Another similar front structure is AZO (Al doped ZnO) nanorods which experimentally provided a front surface reflectance of about 12% at 400-900 nm wavelength [171].

Saravanan *et al.* designed a 1-D photonic crystal (i.e., a distributed Bragg grating) for the rear side of an a-Si PV cell [172]. which consists of alternating layers of Si and SiO_2 has the potential to make the rear side reflectance near perfect, which could increase the J_{sc} of the thin a-Si PV cells. However, it is unclear how rear side contacts could be formed through this dielectric reflector.

Hossain *et al.* have experimentally demonstrated the use of self-assembled Al_2O_3 nanostructures to provide surface passivation and rear-side photon management in c-Si PV cells [94, 149, 173]. They have the potential to achieve high rear side reflectance ($\geq 95\%$), due to the suppression of parasitic optical losses in the metal contacts [160–162]. They indicated that these structures can provide up to 1 mA/cm^2 increase in J_{sc} for cells with Al rear contacts and up to 2.9 mA/cm^2 for Ni contacts. In a similar simulation work by Shameli, a polarization independent phase gradient metasurface was proposed for the rear side of the cell [174]. This structure can provide a rear side reflectance of 83%, but surface recombination at the Si/Al boundary is not addressed, which could negatively impact cell performance.

Dhawan *et al.* proposed using transformation optics to design photon management structures on Si surfaces, recognizing that texturing the surface increases recombination and it may not be possible to fully passivate it [175]. They proposed using optically equivalent planar layers with varying refractive indices instead of a nano-structured surface. However, it remains uncertain how to fabricate these precise planar layers with varying refractive indices.

Sun *et al.* suggested using metallic light-trapping electrodes on the front side of PV cells, which can significantly decrease shadowing loss and have potential for use in front-side metal grids, increasing the active area and overall current of the cell [176–178].

Khokhar *et al.* recently designed a TOPcon cell that incorporates a nanosilicon structure on both sides of the cell [179]. By considering both bulk and surface recombination in their simulation, they were able to achieve a J_{sc} of 43.5 mA/cm^2 , a V_{oc} of 0.762 V and an FF of 83%. These results are slightly higher than those of practical TOPcon cells reported in Table 1, suggesting that there is potential for further improvement in the performance of practical TOPcon cells through improved photon management and advancements in processing techniques that can reduce recombination losses.

6. Conclusion

In conclusion, the front side structure, rear side structure, and thickness of a PV cell are crucial parameters to consider when designing an efficient photon management mechanism. The results of this study suggest that by incorporating a well-passivated nanostructured front side and a dielectric-made rear side that effectively scatters light without impeding current conduction, excellent light trapping can be achieved and an increase in cell J_{sc} , V_{oc} and efficiency can be realized. Additionally, the cell thickness should be optimized such that it is less than the minority carrier diffusion length while still allowing for the capture of a majority of longer wavelength photons. We also explored various contemporary photon management structures that have not yet been implemented in practical PV cells. Some

of these structures demonstrated promising results in terms of light trapping, however, the surface passivation of these structures poses a challenge for their practical use in PV cells.

Acknowledgments

This material is based upon work supported by the U.S. Department of Energy's Office of Energy Efficiency and Renewable Energy (EERE) under the Solar Energy Technologies Office Agreement Number DE-EE0007533. The authors would like to acknowledge Prof. Pieter G. Kik for his insightful discussions and valuable perspectives that significantly enhanced the quality of this work. During the preparation of this work, the authors used ChatGPT in order to correct grammatical errors in some parts of the manuscript. After using this tool/service, the authors reviewed and edited the content as needed and take full responsibility for the content of the publication.

Data Availability

Datasets related to this article can be found at <https://doi.org/10.6084/m9.figshare.23573409>, an open source online data repository hosted at figshare [180].

References

- [1] J. Ellsmoor, Renewable energy is now the cheapest option - even without subsidies, 2019. URL: <https://www.forbes.com/sites/jamesellsmoor/2019/06/15/renewable-energy-is-now-the-cheapest-option-eve>
- [2] S. Philipps, W. Warmuth, Photovoltaics report, Fraunhofer Institute for Solar Energy Systems, ISE (2020). URL: <https://www.ise.fraunhofer.de/content/dam/ise/de/documents/publications/studies/Photovoltaics-Re>
- [3] Photovoltaic Degradation Rates—an Analytical Review 21(????). URL: <https://onlinelibrary.wiley.com/doi/abs/10.1002/pip.1182>. doi:10.1002/pip.1182.
- [4] K. O. Davis, S. R. Kurtz, D. C. Jordan, J. H. Wohlgemuth, N. Sorloaica-Hickman, Multipronged analysis of degradation rates of photovoltaic modules and arrays deployed in Florida, Progress in Photovoltaics: Research and Applications 21 (2013) 702–712. URL: <http://onlinelibrary.wiley.com/doi/10.1002/pip.2154/abstract>. doi:10.1002/pip.2154, number: 4.
- [5] D. C. Jordan, S. R. Kurtz, K. VanSant, J. Newmiller, Compendium of photovoltaic degradation rates, Progress in Photovoltaics: Research and Applications 24 (2016) 978–989. doi:10.1002/pip.2744, number: 7.
- [6] D. C. Jordan, B. Marion, C. Deline, T. Barnes, M. Bolinger, PV field reliability status—Analysis of 100 000 solar systems, Progress in Photovoltaics: Research and Applications 28 (2020) 739–754. URL: <http://onlinelibrary.wiley.com/doi/abs/10.1002/pip.3262>. doi:10.1002/pip.3262, number: 8 eprint: <https://onlinelibrary.wiley.com/doi/pdf/10.1002/pip.3262>.
- [7] R. Jones-Albertus, D. Feldman, R. Fu, K. Horowitz, M. Woodhouse, Technology advances needed for photovoltaics to achieve widespread grid price parity, Progress in photovoltaics: research and applications 24 (2016) 1272–1283.
- [8] At 26.81%, longi sets a new world record efficiency for silicon solar cells, ????. URL: <https://www.longi.com/en/news/propelling-the-transformation/>.
- [9] Best research-cell efficiency chart, ????. URL: <https://www.nrel.gov/pv/assets/pdfs/cell-pv-eff-crysi.pdf>.
- [10] A. Richter, M. Hermle, S. W. Glunz, Reassessment of the limiting efficiency for crystalline silicon solar cells, IEEE Journal of Photovoltaics 3 (2013) 1184–1191. doi:10.1109/JPHOTOV.2013.2270351.
- [11] S. Jeong, S. Wang, Y. Cui, Nanoscale photon management in silicon solar cells, Journal of Vacuum Science & Technology A 30 (2012) 060801. URL: <https://doi.org/10.1116/1.4759260>. doi:10.1116/1.4759260. arXiv:<https://doi.org/10.1116/1.4759260>.
- [12] A. Peter Amalathas, M. M. Alkai, Nanostructures for light trapping in thin film solar cells, Micromachines 10 (2019). URL: <https://www.mdpi.com/2072-666X/10/9/619>. doi:10.3390/mi10090619.
- [13] V. K. Narasimhan, Y. Cui, Nanostructures for photon management in solar cells, Nanophotonics 2 (2013) 187–210. URL: <https://doi.org/10.1515/nanoph-2013-0001>. doi:doi:10.1515/nanoph-2013-0001.

- [14] H.-P. Wang, D.-H. Lien, M.-L. Tsai, C.-A. Lin, H.-C. Chang, K.-Y. Lai, J.-H. He, Photon management in nanostructured solar cells, *J. Mater. Chem. C* 2 (2014) 3144–3171. URL: <http://dx.doi.org/10.1039/C3TC32067G>. doi:10.1039/C3TC32067G.
- [15] R. Saive, Light trapping in thin silicon solar cells: A review on fundamentals and technologies, *Progress in Photovoltaics: Research and Applications* 29 (2021) 1125–1137. URL: <https://onlinelibrary.wiley.com/doi/abs/10.1002/pip.3440>. doi:<https://doi.org/10.1002/pip.3440>. arXiv:<https://onlinelibrary.wiley.com/doi/pdf/10.1002/pip.3440>.
- [16] C. Battaglia, A. Cuevas, S. De Wolf, High-efficiency crystalline silicon solar cells: status and perspectives, *Energy & Environmental Science* (2016). doi:10.1039/c5ee03380b.
- [17] J. Liu, Y. Yao, S. Xiao, X. Gu, Review of status developments of high-efficiency crystalline silicon solar cells, *Journal of Physics D: Applied Physics* 51 (2018) 123001. URL: <https://doi.org/10.1088/1361-6463/aaac6d>. doi:10.1088/1361-6463/aaac6d, publisher: IOP Publishing.
- [18] H. Steinkemper, M. Hermle, S. W. Glunz, Comprehensive simulation study of industrially relevant silicon solar cell architectures for an optimal material parameter choice, *Progress in Photovoltaics: Research and Applications* (2016). doi:10.1002/pip.2790.
- [19] R. Jaiswal, M. Mart´inez-Ram´on, T. Busani, Recent advances in silicon solar cell research using data sciencebased learning, *IEEE Journal of Photovoltaics* (2022).
- [20] E. Vazsonyi, K. De Clercq, R. Einhaus, E. Van Kerschaver, K. Said, J. Poortmans, J. Szlufcik, J. Nijs, Improved anisotropic etching process for industrial texturing of silicon solar cells, *Solar energy materials and solar cells* 57 (1999) 179–188.
- [21] P. Papet, O. Nichiporuk, A. Kaminski, Y. Rozier, J. Kraiem, J.-F. Lelievre, A. Chaumartin, A. Fave, M. Lemiti, Pyramidal texturing of silicon solar cell with tmah chemical anisotropic etching, *Solar Energy Materials and Solar Cells* 90 (2006) 2319–2328.
- [22] K. R. McIntosh, L. P. Johnson, Recombination at textured silicon surfaces passivated with silicon dioxide, *Journal of applied physics* 105 (2009) 124520.
- [23] D. H. Macdonald, A. Cuevas, M. J. Kerr, C. Samundsett, D. Ruby, S. Winderbaum, A. Leo, Texturing industrial multicrystalline silicon solar cells, *Solar Energy* 76 (2004) 277–283. URL: <http://www.sciencedirect.com/science/article/pii/S0038092X03003128>. doi:10.1016/j.solener.2003.08.019.
- [24] S. C. Baker-Finch, K. R. McIntosh, M. L. Terry, W. Yimao, Isotextured Silicon Solar Cell Analysis and Modeling 2: Recombination and Device Modeling, *IEEE Journal of Photovoltaics* 2 (2012) 465–472. doi:10.1109/JPHOTOV.2012.2204390.
- [25] S. C. Baker-Finch, K. R. McIntosh, M. L. Terry, Isotextured Silicon Solar Cell Analysis and Modeling 1: Optics, *Photovoltaics, IEEE Journal of* 2 (2012) 457–464. doi:10.1109/JPHOTOV.2012.2206569.
- [26] K. Sreejith, A. K. Sharma, P. K. Basu, A. Kottantharayil, Etching methods for texturing industrial multi-crystalline silicon wafers: A comprehensive review, *Solar Energy Materials and Solar Cells* 238 (2022) 111531. URL: <https://www.sciencedirect.com/science/article/pii/S0927024821005675>. doi:<https://doi.org/10.1016/j.solmat.2021.111531>.
- [27] B. Vermang, A. Rothschild, K. Kenis, K. Wostyn, T. Bearda, A. Racz, X. Loozen, J. John, P. W. Mertens, J. Poortmans, et al., Surface passivation for si solar cells: a combination of advanced surface cleaning and thermal atomic layer deposition of al₂o₃, in: *Solid State Phenomena*, volume 187, Trans Tech Publ, 2012, pp. 357–361.
- [28] A. Moldovan, K. Birmann, J. Rentsch, M. Zimmer, T. Gitte, J. Fittkau, Combined Ozone/HF/HCl based cleaning and adjusted emitter etch-back for silicon solar cells, *Solid State Phenomena* 195 (2013) 305–309. doi:10.4028/www.scientific.net/SSP.195.305.
- [29] I. Kuzma-Filipek, M. Recaman-Payo, M. Aleman, J. John, M. Haslinger, E. Cornagliotti, F. Duerinckx, A. Hajjiah, M. Soha, R. Russel, A. Sharma, A. Uruena, J. Szlufcik, I. Gordon, Simplified cleaning for 22.5% nPERT solar cells with rear epitaxial emitters, *Solar Energy Materials and Solar Cells* (2016).doi:10.1016/j.solmat.2016.06.036.
- [30] H. Ali, A. Moldovan, S. Mack, M. Wilson, W. V. Schoenfeld, K. O. Davis, Influence of surface preparation and cleaning on the passivation of boron diffused silicon surfaces for high efficiency photovoltaics, *Thin Solid Films* 636 (2017) 412–418. doi:10.1016/j.tsf.2017.06.043.
- [31] A. B. Morales-Vilches, E.-C. Wang, T. Henschel, M. Kubicki, A. Cruz, S. Janke, L. Korte, R. Schlatmann, B. Stannowski, Improved Surface Passivation by Wet Texturing, Ozone-Based Cleaning, and Plasma-Enhanced Chemical Vapor Deposition Processes for High-Efficiency Silicon Heterojunction Solar Cells, *physica status solidi (a)* 217 (2020) 1900518. URL: <https://onlinelibrary.wiley.com/doi/abs/10.1002/pssa.201900518>. doi:10.1002/pssa.201900518, eprint: <https://onlinelibrary.wiley.com/doi/pdf/10.1002/pssa.201900518>.
- [32] A. Moldovan, F. Feldmann, G. Krugel, M. Zimmer, J. Rentsch, M. Hermle, A. Roth-Fölsch, K. Kaufmann, C. Hagendorf, Simple cleaning and conditioning of silicon surfaces with uv/ozone sources, *Energy Procedia* 55 (2014) 834–844.
- [33] S. Bakhshi, N. Zin, H. Ali, M. Wilson, D. Chanda, K. O. Davis, W. V. Schoenfeld, Simple and versatile uv-ozone oxide for silicon solar cell applications, *Solar Energy Materials and Solar Cells* 185 (2018) 505–510.
- [34] M. Z. Rahman, Advances in surface passivation and emitter optimization techniques of c-Si solar cells, *Renewable and Sustainable Energy Reviews* 30 (2014) 734–742. doi:10.1016/j.rser.2013.11.025.
- [35] H. Hieslmair, L. Mandrell, I. Latchford, M. Chun, J. Sullivan, B. Adibi, High throughput ion-implantation for silicon solar cells, *Energy Procedia* 27 (2012) 122–128.
- [36] A. Rohatgi, D. L. Meier, B. McPherson, Y.-W. Ok, A. D. Upadhyaya, J.-H. Lai, F. Zimbardi, High-throughput ion-implantation for low-cost high-efficiency silicon solar cells, *Energy Procedia* 15 (2012) 10–19.

- [37] K. O. Davis, K. Jiang, C. Demberger, H. Zunft, H. Haverkamp, D. Habermann, W. V. Schoenfeld, Improved control of the phosphorus surface concentration during in-line diffusion of c-si solar cells by apcvd, *physica status solidi (RRL)*–Rapid Research Letters 7 (2013) 319–321.
- [38] P. Rothhardt, C. Demberger, A. Wolf, D. Biro, Co-diffusion from apcvd bsg and pocl3 for industrial n-type solar cells, *Energy Procedia* 38 (2013) 305–311.
- [39] H. Wagner, A. Dastgheib-Shirazi, B. Min, A. E. Morishige, M. Steyer, G. Hahn, C. del Canizo, T. Buonassisi, P. P. Altermatt, Optimizing phosphorus diffusion for photovoltaic applications: Peak doping, inactive phosphorus, gettering, and contact formation, *Journal of Applied Physics* 119 (2016) 185704.
- [40] A. G. Aberle, Overview on SiN surface passivation of crystalline silicon solar cells, *Solar Energy Materials and Solar Cells* 65 (2001) 239–248. doi:[http://dx.doi.org/10.1016/S0927-0248\(00\)00099-4](http://dx.doi.org/10.1016/S0927-0248(00)00099-4).
- [41] A. G. Aberle, Surface Passivation of Crystalline Silicon Solar Cells: A Review, *Progress in Photovoltaics: Research and Applications* 8 (2000) 473–487. doi:10.1002/1099-159X(200009/10)8:5<473::AID-PIP337>3.0.CO;2D.
- [42] A. Cuevas, Y. Wan, D. Yan, C. Samundsett, T. Allen, X. Zhang, J. Cui, J. Bullock, Carrier population control and surface passivation in solar cells, *Solar Energy Materials and Solar Cells* 184 (2018) 38–47. URL: <http://www.sciencedirect.com/science/article/pii/S0927024818302010>. doi:10.1016/j.solmat.2018.04.026.
- [43] G. Dingemans, W. M. M. Kessels, Status and prospects of Al₂O₃-based surface passivation schemes for silicon solar cells, *Journal of Vacuum Science & Technology A: Vacuum, Surfaces, and Films* 30 (2012) 040802–1– 040802–27. doi:10.1116/1.4728205.
- [44] M. Rahman, S. Khan, Advances in surface passivation of c-Si solar cells, *Materials for Renewable and Sustainable Energy* 1 (2012) 1–11. doi:10.1007/s40243-012-0001-y.
- [45] R. S. Bonilla, B. Hoex, P. Hamer, P. R. Wilshaw, Dielectric surface passivation for silicon solar cells: A review: Dielectric surface passivation for silicon solar cells, *physica status solidi (a)* 214 (2017) 1700293. URL: <http://doi.wiley.com/10.1002/pssa.201700293>. doi:10.1002/pssa.201700293.
- [46] C. Ballif, D. Huljić, G. Willeke, A. Hessler-Wyser, Silver thick-film contacts on highly doped n-type silicon emitters: structural and electronic properties of the interface, *Applied physics letters* 82 (2003) 1878–1880.
- [47] G. Schubert, F. Huster, P. Fath, Physical understanding of printed thick-film front contacts of crystalline si solar cells—review of existing models and recent developments, *Solar energy materials and solar cells* 90 (2006) 3399–3406.
- [48] A. Ebong, N. Chen, Metallization of crystalline silicon solar cells: A review, in: *High Capacity Optical Networks and Emerging/Enabling Technologies*, 2012, pp. 102–109. doi:10.1109/HONET.2012.6421444.
- [49] A. Kaminski, B. Vandelle, A. Fave, J. P. Boyeaux, L. Quan Nam, R. Monna, D. Sarti, A. Laugier, Aluminium BSF in silicon solar cells, *Solar Energy Materials & Solar Cells* 72 (2002) 373–379.
- [50] J. D. Fields, M. I. Ahmad, V. L. Pool, J. Yu, D. G. Van Campen, P. A. Parilla, M. F. Toney, M. F. A. M. van Hest, The formation mechanism for printed silver-contacts for silicon solar cells, *Nature Communications* 7 (2016) 11143. URL: <https://www.nature.com/articles/ncomms11143>. doi:10.1038/ncomms11143.
- [51] V. Shanmugam, J. Wong, I. M. Peters, J. Cunnusamy, M. Zahn, A. Zhou, R. Yang, X. Chen, A. G. Aberle, T. Mueller, Analysis of Fine-Line Screen and Stencil-Printed Metal Contacts for Silicon Wafer Solar Cells, *IEEE Journal of Photovoltaics* 5 (2015) 525–533. doi:10.1109/JPHOTOV.2014.2388073.
- [52] J. Zhang, H. Tong, X. Sun, G. Li, H. Li, Y. Yang, X. Yuan, C. Liu, H. Li, An investigation on determinants of silver paste metallization contact performance on crystalline silicon solar cells, *Journal of Materials Science: Materials in Electronics* (2020). URL: <https://doi.org/10.1007/s10854-020-03145-9>. doi:10.1007/s10854020-03145-9.
- [53] S. Xiong, X. Yuan, Y. Yang, J. Zhang, H. Tong, C. Liu, X. Ye, S. Li, L. Luo, X. Wang, Macroscopic Study on Current Transport Path in Front-Side Contacts of Crystalline Silicon Solar Cells, *physica status solidi (a)* 0 (????) 1900480. URL: <https://onlinelibrary.wiley.com/doi/abs/10.1002/pssa.201900480>. doi:10.1002/pssa.201900480.
- [54] S. Tepner, N. Wengenmeyr, M. Linse, A. Lorenz, M. Pospischil, F. Clement, The Link between AgPaste Rheology and Screen-Printed Solar Cell Metallization, *Advanced Materials Technologies* 5 (2020) 2000654. URL: <https://www.onlinelibrary.wiley.com/doi/abs/10.1002/admt.202000654>. doi:<https://doi.org/10.1002/admt.202000654>, eprint: <https://onlinelibrary.wiley.com/doi/pdf/10.1002/admt.202000654>.
- [55] E. J. Schneller, M. J. Hossain, R. Frota, A. J. Curran, M. Wang, J.-N. Jaubert, J. L. Braid, R. H. French, K. O. Davis, Performance evaluation of commercially relevant p-type silicon cell architectures, in: *2019 IEEE 46th Photovoltaic Specialists Conference (PVSC)*, 2019, pp. 0326–0329. doi:10.1109/PVSC40753.2019.8980618.
- [56] M. J. Hossain, G. Gregory, H. Patel, S. Guo, E. J. Schneller, A. M. Gabor, Z. Yang, A. L. Blum, K. O. Davis, Detailed performance loss analysis of silicon solar cells using high-throughput metrology methods, in: *2018 IEEE 7th World Conference on Photovoltaic Energy Conversion (WCPEC) (A Joint Conference of 45th IEEE PVSC, 28th PVSEC 34th EU PVSEC)*, 2018, pp. 2214–2218. doi:10.1109/PVSC.2018.8547869.
- [57] A. W. Blakers, A. Wang, A. M. Milne, J. Zhao, M. A. Green, 22.8% efficient silicon solar cell, *Applied Physics Letters* 55 (1989) 1363–1365. URL: <https://doi.org/10.1063/1.101596>. doi:10.1063/1.101596. arXiv:<https://doi.org/10.1063/1.101596>.
- [58] M. A. Green, A. W. Blakers, J. Zhao, A. M. Milne, A. Wang, X. Dai, Characterization of 23-% efficient silicon solar cells, *IEEE Transactions on Electron Devices* 37 (1990) 331–336.

- [59] A. Blakers, Development of the perc solar cell, *IEEE Journal of Photovoltaics* 9 (2019) 629–635.
- [60] T. Dullweber, J. Schmidt, Industrial Silicon Solar Cells Applying the Passivated Emitter and Rear Cell (PERC) Concept—A Review, *IEEE Journal of Photovoltaics* 6 (2016) 1366–1381. doi:10.1109/JPHOTOV.2016.2571627.
- [61] B. Min, M. Müller, H. Wagner, G. Fischer, R. Brendel, P. P. Altermatt, H. Neuhaus, A Roadmap Toward 24% Efficient PERC Solar Cells in Industrial Mass Production, *IEEE Journal of Photovoltaics* 7 (2017) 1541–1550. doi:10.1109/JPHOTOV.2017.2749007.
- [62] S. D. Wolf, A. Descoeurdes, Z. C. Holman, C. Ballif, High-efficiency silicon heterojunction solar cells: A review, *Green* 2 (2012) 7–24. URL: <https://doi.org/10.1515/green-2011-0018>. doi:doi:10.1515/green-2011-0018.
- [63] A. Razaq, T. G. Allen, W. Liu, Z. Liu, S. De Wolf, Silicon heterojunction solar cells: Techno-economic assessment and opportunities, *Joule* 6 (2022) 514–542. URL:<https://www.sciencedirect.com/science/article/pii/S2542435122000903>. doi:<https://doi.org/10.1016/j.joule.2022.02.009>.
- [64] M. Taguchi, Review—development history of high efficiency silicon heterojunction solar cell: From discovery to practical use, *ECS Journal of Solid State Science and Technology* 10 (2021) 025002. URL: <https://dx.doi.org/10.1149/2162-8777/abdfb6>. doi:10.1149/2162-8777/abdfb6.
- [65] A. Louwen, W. van Sark, R. Schropp, A. Faaij, A cost roadmap for silicon heterojunction solar cells, *Solar Energy Materials and Solar Cells* 147 (2016) 295–314. doi:10.1016/j.solmat.2015.12.026.
- [66] J. Haschke, O. Dupré, M. Boccard, C. Ballif, Silicon heterojunction solar cells: Recent technological development and practical aspects - from lab to industry, *Solar Energy Materials and Solar Cells* 187 (2018) 140–153. URL: <http://www.sciencedirect.com/science/article/pii/S0927024818303805>. doi:10.1016/j.solmat.2018.07.018.
- [67] Y. Liu, Y. Li, Y. Wu, G. Yang, L. Mazzarella, P. Procel-Moya, A. C. Tamboli, K. Weber, M. Boccard, O. Isabella, X. Yang, B. Sun, High-Efficiency Silicon Heterojunction Solar Cells: Materials, Devices and Applications, *Materials Science and Engineering: R: Reports* 142 (2020) 100579. URL: <http://www.sciencedirect.com/science/article/pii/S0927796X20300371>. doi:10.1016/j.mser.2020.100579.
- [68] E. Yablonovitch, T. Gmitter, R. M. Swanson, Y. H. Kwark, A 720 mV open circuit voltage SiO_x:c-Si:SiO_x double heterostructure solar cell, *Applied Physics Letters* 47 (1985) 1211. doi:10.1063/1.96331.
- [69] F. Haase, C. Hollemann, S. Schöfer, A. Merkle, M. Rieñacker, J. Kruñgener, R. Brendel, R. Peibst, Laser contact openings for local poly-si-metal contacts enabling 26.1% efficient polo-ibc solar cells, *Solar Energy Materials and Solar Cells* 186 (2018) 184–193. URL: <https://www.sciencedirect.com/science/article/pii/S0927024818303076>. doi:<https://doi.org/10.1016/j.solmat.2018.06.020>.
- [70] F. Haase, S. Schöfer, C. Klamt, F. Kiefer, J. Kruñgener, R. Brendel, R. Peibst, Perimeter Recombination in 25% Efficient IBC Solar Cells With Passivating POLO Contacts for Both Polarities, *IEEE Journal of Photovoltaics* 8 (2018) 23–29. doi:10.1109/JPHOTOV.2017.2762592.
- [71] R. Peibst, U. Römer, Y. Larionova, M. Rieñacker, A. Merkle, N. Folchert, S. Reiter, M. Turcu, B. Min, J. Kruñgener, D. Tetzlaff, E. Bugiel, T. Wietler, R. Brendel, Working principle of carrier selective poly-Si/c-Si junctions: Is tunnelling the whole story?, *Solar Energy Materials and Solar Cells* 158 (2016) 60–67. URL: <http://www.sciencedirect.com/science/article/pii/S0927024816301519>. doi:10.1016/j.solmat.2016.05.045.
- [72] S. Duttgupta, N. Nandakumar, P. Padhamnath, J. K. Buatis, R. Stangl, A. G. Aberle, monoPoly™ cells: Large-area crystalline silicon solar cells with fire-through screen printed contact to doped polysilicon surfaces, *Solar Energy Materials and Solar Cells* 187 (2018) 76–81. URL: <http://www.sciencedirect.com/science/article/pii/S092702481830285X>. doi:10.1016/j.solmat.2018.05.059.
- [73] P. Padhamnath, J. Wong, B. Nagarajan, J. K. Buatis, L. M. Ortega, N. Nandakumar, A. Khanna, V. Shanmugam, S. Duttgupta, Metal contact recombination in monoPoly™ solar cells with screen-printed & fire-through contacts, *Solar Energy Materials and Solar Cells* 192 (2019) 109–116. URL: <http://www.sciencedirect.com/science/article/pii/S0927024818305919>. doi:10.1016/j.solmat.2018.12.026.
- [74] F. Feldmann, M. Bivour, C. Reichel, M. Hermle, S. W. Glunz, Passivated rear contacts for high-efficiency n-type Si solar cells providing high interface passivation quality and excellent transport characteristics, *Solar Energy Materials and Solar Cells* 120 (2014) 270–274. URL: <http://www.sciencedirect.com/science/article/pii/S0927024813004868>. doi:10.1016/j.solmat.2013.09.017.
- [75] F. Feldmann, M. Bivour, C. Reichel, H. Steinkemper, M. Hermle, S. W. Glunz, Tunnel oxide passivated contacts as an alternative to partial rear contacts, *Solar Energy Materials and Solar Cells* 131 (2014) 46–50. URL: <http://www.sciencedirect.com/science/article/pii/S0927024814003249>. doi:10.1016/j.solmat.2014.06.015.
- [76] Y. Chen, D. Chen, C. Liu, Z. Wang, Y. Zou, Y. He, Y. Wang, L. Yuan, J. Gong, W. Lin, X. Zhang, Y. Yang, H. Shen, Z. Feng, P. P. Altermatt, P. J. Verlinden, Mass production of industrial tunnel oxide passivated contacts (i-TOPCon) silicon solar cells with average efficiency over 23% and modules over 345 W, *Progress in Photovoltaics: Research and Applications* 27 (2019) 827–834. URL: <https://onlinelibrary.wiley.com/doi/abs/10.1002/pip.3180>. doi:10.1002/pip.3180.
- [77] D. Chen, Y. Chen, Z. Wang, J. Gong, C. Liu, Y. Zou, Y. He, Y. Wang, L. Yuan, W. Lin, R. Xia, L. Yin, X. Zhang, G. Xu, Y. Yang, H. Shen, Z. Feng, P. P. Altermatt, P. J. Verlinden, 24.58% total area efficiency of screen-printed, large area industrial silicon solar cells with the tunnel oxide passivated contacts (i-TOPCon) design, *Solar Energy Materials and Solar Cells* 206 (2020) 110258. URL: <http://www.sciencedirect.com/science/article/pii/S0927024819305872>. doi:10.1016/j.solmat.2019.110258.

- [78] B. Kafle, B. S. Goraya, S. Mack, F. Feldmann, S. Nold, J. Rentsch, TOPCon – Technology options for cost efficient industrial manufacturing, *Solar Energy Materials and Solar Cells* 227 (2021) 111100. URL: <https://www.sciencedirect.com/science/article/pii/S0927024821001422>. doi:10.1016/j.solmat.2021.111100.
- [79] D. K. Ghosh, S. Bose, G. Das, S. Acharyya, A. Nandi, S. Mukhopadhyay, A. Sengupta, Fundamentals, present status and future perspective of topcon solar cells: A comprehensive review, *Surfaces and Interfaces* 30 (2022) 101917. URL: <https://www.sciencedirect.com/science/article/pii/S2468023022001973>. doi:<https://doi.org/10.1016/j.surfin.2022.101917>.
- [80] E. V. Kerschaver, G. Beaucarne, Back-contact solar cells: A review, *Progress in Photovoltaics: Research and Applications* 14 (2006) 107–123.
- [81] M. M. Desa, S. Sapeai, A. Azhari, K. Sopian, M. Sulaiman, N. Amin, S. Zaidi, Silicon back contact solar cell configuration: A pathway towards higher efficiency, *Renewable and sustainable energy reviews* 60 (2016) 1516–1532.
- [82] Q. Pengcheng, Q. Pengxiang, Characteristics and development of interdigital back contact solar cells, *IOP Conference Series: Earth and Environmental Science* 621 (2021) 012067. URL: <https://dx.doi.org/10.1088/1755-1315/621/1/012067>. doi:10.1088/1755-1315/621/1/012067.
- [83] M. J. Hossain, G. Gregory, E. J. Schneller, A. M. Gabor, A. L. Blum, Z. Yang, D. Sulas, S. Johnston, K. O. Davis, A comprehensive methodology to evaluate losses and process variations in silicon solar cell manufacturing, *IEEE Journal of Photovoltaics* 9 (2019) 1350–1359. doi:10.1109/JPHOTOV.2019.2926628.
- [84] E. J. Schneller, M. J. Hossain, R. Frota, N. Iqbal, D. Colvin, A. J. Curran, M. Wang, J. L. Braid, L. S. Bruckman, R. H. French, B. D. Huey, J. N. Jaubert, K. O. Davis, Spatially resolved characterization of optical and recombination losses for different industrial silicon solar cell architectures, *International Journal of Modern Physics B* 34 (2020) 2050204–3. doi:10.1142/S0217979220502045.
- [85] K. Wijekoon, F. Yan, Y. Zheng, D. Wang, H. Mungekar, L. Zhang, H. Ponnekanti, Optimization of rear local contacts on high efficiency perc solar cells structures, *International Journal of Photoenergy* 2013 (2013). URL: <https://www.hindawi.com/journals/ijp/2013/368403/>. doi:10.1155/2013/368403.
- [86] M. J. Hossain, G. Gregory, E. Schneller, K. Davis, Dataset - a comprehensive methodology to evaluate losses and process variations in silicon solar cell manufacturing, 2019. URL: https://figshare.com/articles/dataset/Dataset - A Comprehensive _Methodology to Evaluate Losses and Proc doi:10.6084/m9.figshare.7636922.v2.
- [87] L. Zeng, Y. Yi, C. Hong, J. Liu, N. Feng, X. Duan, L. C. Kimerling, B. A. Alamariu, Efficiency enhancement in si solar cells by textured photonic crystal back reflector, *Applied Physics Letters* 89 (2006) 111111. URL: <https://doi.org/10.1063/1.2349845>. doi:10.1063/1.2349845. arXiv:<https://doi.org/10.1063/1.2349845>.
- [88] S. Bhattacharya, S. John, Beyond 30% conversion efficiency in silicon solar cells: A numerical demonstration, *Scientific Reports* 9 (2019) 2045–2322. URL: <https://www.nature.com/articles/s41598-019-48981-w>. doi:10.1038/s41598-019-48981-w.
- [89] J. Nelson, *The Physics of Solar Cells*, PUBLISHED BY IMPERIAL COLLEGE PRESS AND DISTRIBUTED BY WORLD SCIENTIFIC PUBLISHING CO., 2003.
URL: <https://www.worldscientific.com/doi/abs/10.1142/p276>. doi:10.1142/p276. arXiv:<https://www.worldscientific.com/doi/pdf/10.1142/p276>.
- [90] R. Biswas, J. Bhattacharya, B. Lewis, N. Chakravarty, V. Dalal, Enhanced nanocrystalline silicon solar cell with a photonic crystal back-reflector, *Solar Energy Materials and Solar Cells* 94 (2010) 2337 – 2342. URL: <http://www.sciencedirect.com/science/article/pii/S0927024810004642>. doi:<https://doi.org/10.1016/j.solmat.2010.08.007>.
- [91] M. J. Hossain, K. O. Davis, Photon management for silicon solar cells featuring hole-selective molybdenum oxide rear contacts: An optical simulation study, in: *2019 IEEE 46th Photovoltaic Specialists Conference (PVSC)*, 2019, pp. 1901–1905. doi:10.1109/PVSC40753.2019.8981196.
- [92] P. Singh, N. Ravindra, Temperature dependence of solar cell performance—an analysis, *Solar Energy Materials and Solar Cells* 101 (2012) 36–45. URL:<https://www.sciencedirect.com/science/article/pii/S0927024812000931>. doi:<https://doi.org/10.1016/j.solmat.2012.02.019>.
- [93] Y. Kato, S. Fujimoto, M. Kozawa, H. Fujiwara, Maximum efficiencies and performance-limiting factors of inorganic and hybrid perovskite solar cells, *Phys. Rev. Appl.* 12 (2019) 024039. URL: <https://link.aps.org/doi/10.1103/PhysRevApplied.12.024039>. doi:10.1103/PhysRevApplied.12.024039.
- [94] M. J. Hossain, Measurement and mitigation of optical, recombination and resistive losses in silicon photovoltaics, *Electronic Theses and Dissertations* (2021). URL: <https://stars.library.ucf.edu/etd2020/1495>.
- [95] B. Vermang, H. Goverde, A. Uruena, A. Lorenz, E. Cornagliotti, A. Rothschild, J. John, J. Poortmans, R. Mertens, Blistering in ald al2o3 passivation layers as rear contacting for local al bsf si solar cells, *Solar Energy Materials and Solar Cells* 101 (2012) 204–209. URL: <http://www.sciencedirect.com/science/article/pii/S0927024812000487>. doi:<https://doi.org/10.1016/j.solmat.2012.01.032>.
- [96] A. Volk, N. Tucher, J. Seiffe, H. Hauser, M. Zimmer, B. Bl'asi, M. Hofmann, J. Rentsch, Honeycomb structure on multi-crystalline silicon al-bsf solar cell with 17.8% efficiency, *IEEE Journal of Photovoltaics* 5 (2015) 1027–1033. doi:10.1109/JPHOTOV.2015.2402757.
- [97] H.-P. Wang, J.-H. He, Toward highly efficient nanostructured solar cells using concurrent electrical and optical design, *Advanced Energy Materials* 7 (????) 1602385. URL:<https://onlinelibrary.wiley.com/doi/abs/10.1002/aenm.201602385>. doi:<https://doi.org/10.1002/aenm.201602385>. arXiv:<https://onlinelibrary.wiley.com/doi/pdf/10.1002/aenm.2016>
- [98] S. Jeong, M. D. McGehee, Y. Cui, All-back-contact ultra-thin silicon nanocone solar cells with 13.7% power conversion efficiency, *Nature Communications* 4 (2013). doi:<https://doi.org/10.1038/ncomms3950>.

- [99] K. Lee, I. Hwang, N. Kim, D. Choi, H.-D. Um, S. Kim, K. Seo, 17.6% efficient radial junction solar cells using silicon nano/micro hybrid structures, *Nanoscale* 8 (2016) 14473–14479. URL: <http://dx.doi.org/10.1039/C6NR04611H>. doi:10.1039/C6NR04611H.
- [100] B. Kafle, A. Mannan, T. Freund, L. Clochard, E. Duffy, M. Hofmann, J. Rentsch, R. Preu, Nanotextured multicrystalline al-bsf solar cells reaching 18% conversion efficiency using industrially viable solar cell processes, *physica status solidi (RRL) – Rapid Research Letters* 9 (2015) 448–452. URL: <https://onlinelibrary.wiley.com/doi/abs/10.1002/pssr.201510219>. doi:<https://doi.org/10.1002/pssr.201510219>. arXiv:<https://onlinelibrary.wiley.com/doi/pdf/10.1002/pssr.20151>
- [101] T. Fellmeth, S. Mack, J. Bartsch, D. Erath, U. Jäger, R. Preu, F. Clement, D. Biro, 20.1% efficient silicon solar cell with aluminum back surface field, *IEEE Electron Device Letters* 32 (2011) 1101–1103. doi:10.1109/LED.2011.2157656.
- [102] H. Savin, P. Repo, G. von Gastrow, P. von Gastrow, E. Calle, M. Garín, R. Alcubilla, Black silicon solar cells with interdigitated back-contacts achieve 22.1% efficiency, *Nature Nanotechnology* 10 (2015) 624–628. doi:10.1038/nnano.2015.89.
- [103] Y. Yao, J. Yao, V. K. Narasimhan, Z. Ruan, C. Xie, S. Fan, Y. Cui, Broadband light management using low-q whispering gallery modes in spherical nanoshells, *Nature Communications* 3 (2012). doi:10.1038/ncomms1664.
- [104] K. Yoshikawa, H. Kawasaki, W. Yoshida, T. Irie, K. Konishi, K. Nakano, T. Uto, D. Adachi, M. Kanematsu, H. Uzu, K. Yamamoto, Silicon heterojunction solar cell with interdigitated back contacts for a photoconversion efficiency over 26%, *Nature Energy* 2 (2017). doi:10.1038/nenergy.2017.32.
- [105] K. Masuko, M. Shigematsu, T. Hashiguchi, D. Fujishima, M. Kai, N. Yoshimura, T. Yamaguchi, Y. Ichihashi, T. Mishima, N. Matsubara, T. Yamanishi, T. Takahama, M. Taguchi, E. Maruyama, S. Okamoto, Achievement of more than 25% conversion efficiency with crystalline silicon heterojunction solar cell, *IEEE Journal of Photovoltaics* 4 (2014) 1433–1435. doi:10.1109/JPHOTOV.2014.2352151.
- [106] D. D. Smith, G. Reich, M. Baldrias, M. Reich, N. Boitnott, G. Bunea, Silicon solar cells with total area efficiency above 25%, in: 2016 IEEE 43rd Photovoltaic Specialists Conference (PVSC), 2016, pp. 3351–3355. doi:10.1109/PVSC.2016.7750287.
- [107] D. Adachi, J. Hernández, K. Yamamoto, Impact of carrier recombination on fill factor for large area heterojunction crystalline silicon solar cell with 25.1% efficiency, *Applied Physics Letters* 107 (2015) 233506. doi:10.1063/1.4937224.
- [108] M. Taguchi, A. Yano, S. Tohoda, K. Matsuyama, Y. Nakamura, T. Nishiwaki, K. Fujita, E. Maruyama, 24.7% record efficiency hit solar cell on thin silicon wafer, *IEEE Journal of Photovoltaics* 4 (2014) 96–99. doi:10.1109/JPHOTOV.2013.2282737.
- [109] X. Li, J. Li, T. Chen, B. Tay, J. Wang, H. Yu, Periodically aligned si nanopillar arrays as efficient antireflection layers for solar cell applications, *Nanoscale Research Letters* 5 (2010). doi:10.1007/s11671-010-9701-3.
- [110] W.-C. Tu, Y.-T. Chang, H.-P. Wang, C.-H. Yang, C.-T. Huang, J.-H. He, S.-C. Lee, Improved light scattering and surface plasmon tuning in amorphous silicon solar cells by double-walled carbon nanotubes, *Solar Energy Materials and Solar Cells* 101 (2012) 200–203. URL: <http://www.sciencedirect.com/science/article/pii/S0927024812000542>. doi:10.1016/j.solmat.2012.01.038.
- [111] D. Yang, F. Lang, Z. Xu, J. Shi, G. Li, Z. Hu, J. Xiong, Influence of atomic layer deposition al₂O₃ nanolayer on the surface passivation of silicon solar cells, *Journal of Semiconductors* 35 (2014) 052002. URL: <https://doi.org/10.1088/1674-4926/35/5/052002>. doi:10.1088/1674-4926/35/5/052002.
- [112] C. Lin, K. Lai, W. Lien, J. He, An efficient broadband and omnidirectional light-harvesting scheme employing a hierarchical structure based on a zno nanorod/si₃n₄-coated si microgroove on 5-inch single crystalline si solar cells, *Nanoscale* (2012). doi:10.1039/C2NR32358C.
- [113] J.-Y. Jung, Z. Guo, S.-W. Jee, H.-D. Um, K.-T. Park, M. S. Hyun, J. M. Yang, J.-H. Lee, A waferscale si wire solar cell using radial and bulk p-n junctions, *Nanotechnology* 21 (2010) 445303. URL: <https://doi.org/10.1088/0957-4484/21/44/445303>. doi:10.1088/0957-4484/21/44/445303.
- [114] K.-Q. Peng, X. Wang, L. Li, X.-L. Wu, S.-T. Lee, High-performance silicon nanohole solar cells, *Journal of the American Chemical Society* 132 (2010) 6872–6873. URL: <https://doi.org/10.1021/ja910082y>. doi:10.1021/ja910082y. arXiv:<https://doi.org/10.1021/ja910082y>, pMID: 20426468.
- [115] E. Garnett, P. Yang, Light trapping in silicon nanowire solar cells, *Nano Letters* 10 (2010) 1082–1087. URL: <https://doi.org/10.1021/nl100161z>. doi:10.1021/nl100161z. arXiv:<https://doi.org/10.1021/nl100161z>, pMID: 20108969.
- [116] B. Tian, X. Zheng, T. Kempa, Y. Fang, N. Yu, G. Yu, J. Huang, C. Lieber, Coaxial silicon nanowires as solar cells and nanoelectronic power sources, *Nature* 449 (2007) 885–889. doi:10.1038/nature06181.
- [117] T. J. Kempa, B. Tian, D. R. Kim, J. Hu, X. Zheng, C. M. Lieber, Single and tandem axial p-i-n nanowire photovoltaic devices, *Nano Letters* 8 (2008) 3456–3460. URL: <https://doi.org/10.1021/nl8023438>. doi:10.1021/nl8023438. arXiv:<https://doi.org/10.1021/nl8023438>, pMID: 18763836.
- [118] E. C. Garnett, P. Yang, Silicon nanowire radial pn junction solar cells, *Journal of the American Chemical Society* 130 (2008) 9224–9225. URL: <https://doi.org/10.1021/ja8032907>. doi:10.1021/ja8032907. arXiv:<https://doi.org/10.1021/ja8032907>, pMID: 18576622.
- [119] J. Zhu, C.-M. Hsu, Z. Yu, S. Fan, Y. Cui, Nanodome solar cells with efficient light management and self-cleaning, *Nano Letters* 10 (2010) 1979–1984. URL: <https://doi.org/10.1021/nl9034237>. doi:10.1021/nl9034237. arXiv:<https://doi.org/10.1021/nl9034237>, pMID: 19891462.
- [120] I. Kuzma-Filipek, K. Nieuwenhuysen, J. Hoeymissen, M. Payo, E. Kerschaver, J. Poortmans, R. Mertens, G. Beaucarne, E. Schmich, S. Lindekugel, S. Reber, Efficiency (>15%) for thinfilm epitaxial silicon solar cells on 70cm² area offspec silicon substrate using porous silicon segmented mirrors, *Progress in Photovoltaics: Research and Applications* 18 (2010) 137–143. URL: <https://onlinelibrary.wiley.com/doi/abs/10.1002/pip.953>. doi:<https://doi.org/10.1002/pip.953>. arXiv:<https://onlinelibrary.wiley.com/doi/pdf/10.1002/pip.953>.

- [121] H. Hannebauer, T. Dullweber, U. Baumann, T. Falcon, R. Brendel, 21.2% efficient fineline-printed perc solar cell with 5 busbar front grid, *physica status solidi (RRL) – Rapid Research Letters* 8 (2014) 675–679. URL: <https://onlinelibrary.wiley.com/doi/abs/10.1002/pssr.201409190>. doi:<https://doi.org/10.1002/pssr.201409190>. arXiv:<https://onlinelibrary.wiley.com/doi/pdf/10.1002/pssr.201409190>
- [122] H. Huang, J. Lv, Y. Bao, R. Xuan, S. Sun, S. Sneek, S. Li, C. Modanese, H. Savin, A. Wang, J. Zhao, 20.8% industrial perc solar cell: Ald al₂o₃ rear surface passivation, efficiency loss mechanisms analysis and roadmap to 24%, *Solar Energy Materials and Solar Cells* 161 (2017) 14 – 30. URL: <http://www.sciencedirect.com/science/article/pii/S0927024816304901>. doi:<https://doi.org/10.1016/j.solmat.2016.11.018>.
- [123] W. Deng, F. Ye, R. Liu, Y. Li, H. Chen, Z. Xiong, Y. Yang, Y. Chen, Y. Wang, P. P. Altermatt, Z. Feng, P. J. Verlinden, 22.61% efficient fully screen printed perc solar cell, in: 2017 IEEE 44th Photovoltaic Specialist Conference (PVSC), 2017, pp. 2220–2226. doi:[10.1109/PVSC.2017.8366416](https://doi.org/10.1109/PVSC.2017.8366416).
- [124] M. Xue, K. N. Nazif, Z. Lyu, J. Jiang, C.-Y. Lu, N. Lee, K. Zang, Y. Chen, T. Zheng, T. I. Kamins, M. L. Brongersma, K. C. Saraswat, J. S. Harris, Free-standing 2.7 m thick ultrathin crystalline silicon solar cell with efficiency above 12.0%, *Nano Energy* 70 (2020) 104466. URL: <https://www.sciencedirect.com/science/article/pii/S2211285520300227>. doi:<https://doi.org/10.1016/j.nanoen.2020.104466>.
- [125] R. Chen, H. Tong, H. Zhu, C. Ding, H. Li, D. Chen, B. Hallam, C. M. Chong, S. Wenham, A. Ciesla, 23.83% efficient mono-perc incorporating advanced hydrogenation, *Progress in Photovoltaics: Research and Applications* 28 (2020) 1239–1247. URL: <https://onlinelibrary.wiley.com/doi/abs/10.1002/pip.3243>. doi:<https://doi.org/10.1002/pip.3243>. arXiv:<https://onlinelibrary.wiley.com/doi/pdf/10.1002/pip.3243>.
- [126] C. Hollemann, F. Haase, S. Schöfer, J. Krügener, R. Brendel, R. Peibst, 26.1% efficient mono-ibc cells: Quantification of electrical and optical loss mechanisms, *Progress in Photovoltaics: Research and Applications* 27 (2019) 950–958. URL: <https://onlinelibrary.wiley.com/doi/abs/10.1002/pip.3098>. doi:<https://doi.org/10.1002/pip.3098>. arXiv:<https://onlinelibrary.wiley.com/doi/pdf/10.1002/pip.3098>.
- [127] M. S. Branham, W.-C. Hsu, S. Yerci, J. Loomis, S. V. Boriskina, B. R. Hoard, S. E. Han, G. Chen, 15.7% efficient 10- μ m-thick crystalline silicon solar cells using periodic nanostructures, *Advanced Materials* 27 (2015) 2182–2188. URL: <https://onlinelibrary.wiley.com/doi/abs/10.1002/adma.201405511>. doi:<https://doi.org/10.1002/adma.201405511>. arXiv:<https://onlinelibrary.wiley.com/doi/pdf/10.1002/adma.201405511>.
- [128] J. H. Petermann, D. Zielke, J. Schmidt, F. Haase, E. G. Rojas, R. Brendel, 19% efficient and 43 μ m-thick crystalline si solar cell from layer transfer using porous silicon, *Progress in Photovoltaics: Research and Applications* 20 (2012) 1–5. URL: <https://onlinelibrary.wiley.com/doi/abs/10.1002/pip.1129>. doi:<https://doi.org/10.1002/pip.1129>. arXiv:<https://onlinelibrary.wiley.com/doi/pdf/10.1002/pip.1129>.
- [129] W. Wang, J. He, D. Yan, C. Samundsett, S. P. Phang, Z. Huang, W. Shen, J. Bullock, Y. Wan, 21.3%-efficient n-type silicon solar cell with a full area rear tio₂/lif/al electron-selective contact, *Solar Energy Materials and Solar Cells* 206 (2020) 110291. URL: <https://www.sciencedirect.com/science/article/pii/S0927024819306208>. doi:<https://doi.org/10.1016/j.solmat.2019.110291>.
- [130] J. Cho, N. Nawal, A. Hadipour, M. Recaman Payo, A. van der Heide, H. S. Radhakrishnan, M. Debucquoy, I. Gordon, J. Szlufcik, J. Poortmans, Interface analysis and intrinsic thermal stability of mox based hole-selective contacts for silicon heterojunction solar cells, *Solar Energy Materials and Solar Cells* 201 (2019) 110074. URL: <https://www.sciencedirect.com/science/article/pii/S0927024819304039>. doi:<https://doi.org/10.1016/j.solmat.2019.110074>.
- [131] X. Yang, E. Aydin, H. Xu, J. Kang, M. Hedhili, W. Liu, Y. Wan, J. Peng, C. Samundsett, A. Cuevas, S. De Wolf, Tantalum nitride electron-selective contact for crystalline silicon solar cells, *Advanced Energy Materials* 8 (2018) 1800608. URL: <https://onlinelibrary.wiley.com/doi/abs/10.1002/aenm.201800608>. doi:<https://doi.org/10.1002/aenm.201800608>. arXiv:<https://onlinelibrary.wiley.com/doi/pdf/10.1002/aenm.201800608>.
- [132] A. Descoeurdes, C. Alleb'e, N. Badel, L. Barraud, J. Champiaud, G. Christmann, F. Debrot, A. Faes, J. Geissbühler, J. Horzel, A. Lachowicz, J. Levrat, S. Martin de Nicolas, S. Nicolay, B. Paviet-Salomon, L.-L. Senaud, C. Ballif, M. Despeisse, Low-temperature processes for passivation and metallization of high-efficiency crystalline silicon solar cells, *Solar Energy* 175 (2018) 54–59. URL: <https://www.sciencedirect.com/science/article/pii/S0038092X18300951>. doi:<https://doi.org/10.1016/j.solener.2018.01.074>, recent Progress in Photovoltaics, Part 1.
- [133] T. G. Allen, J. Bullock, Q. Jeangros, C. Samundsett, Y. Wan, J. Cui, A. Hessler-Wyser, S. De Wolf, A. Javey, A. Cuevas, A low resistance calcium/reduced tania passivated contact for high efficiency crystalline silicon solar cells, *Advanced Energy Materials* 7 (2017) 1602606. URL: <https://onlinelibrary.wiley.com/doi/abs/10.1002/aenm.201602606>. doi:<https://doi.org/10.1002/aenm.201602606>. arXiv:<https://onlinelibrary.wiley.com/doi/pdf/10.1002/aenm.201602606>.
- [134] X. Yang, Q. Bi, H. Ali, K. Davis, W. V. Schoenfeld, K. Weber, High-performance tio₂based electron-selective contacts for crystalline silicon solar cells, *Advanced Materials* 28 (2016) 5891–5897. URL: <https://onlinelibrary.wiley.com/doi/abs/10.1002/adma.201600926>. doi:<https://doi.org/10.1002/adma.201600926>. arXiv:<https://onlinelibrary.wiley.com/doi/pdf/10.1002/adma.201600926>.
- [135] S. Das, M. J. Hossain, S.-F. Leung, A. Lenox, Y. Jung, K. Davis, J.-H. He, T. Roy, A leaf-inspired photon management scheme using optically tuned bilayer nanoparticles for ultra-thin and highly efficient photovoltaic devices, *Nano Energy* 58 (2019) 47–56. URL: <https://www.sciencedirect.com/science/article/pii/S2211285518309856>. doi:<https://doi.org/10.1016/j.nanoen.2018.12.072>.
- [136] F.-I. Lai, J.-F. Yang, Y.-C. Hsu, S.-Y. Kuo, Enhanced conversion efficiency of a-si:h thin-film solar cell using zno nanorods, *Crystals* 10 (2020). URL: <https://www.mdpi.com/2073-4352/10/12/1082>. doi:[10.3390/cryst10121082](https://doi.org/10.3390/cryst10121082).
- [137] Y. Lee, Y. Woo, D.-K. Lee, I. Kim, Fabrication of quasi-hexagonal si nanostructures and its application for flexible crystalline ultrathin si solar cells, *Solar Energy* 208 (2020) 957–965. URL: <https://www.sciencedirect.com/science/article/pii/S0038092X20309026>. doi:<https://doi.org/10.1016/j.solener.2020.08.063>.
- [138] Q. Tang, H. Yao, B. Xu, J. Ge, Enhanced energy conversion efficiency of al-bsf c-si solar cell by a novel hierarchical structure composed of inverted pyramids with different sizes, *Solar Energy* 208 (2020) 1–9. URL: <https://www.sciencedirect.com/science/article/pii/S0038092X20308057>. doi:<https://doi.org/10.1016/j.solener.2020.07.073>.
- [139] C. Huang, K. Sun, W.-L. Chang, Efficiency enhancement of silicon solar cells using a nanoscale honeycomb broadband anti-reflection structure, *Opt. Express* 20 (2012) A85–A93. URL: <http://www.opticsexpress.org/abstract.cfm?URI=oe-20-101-A85>. doi:[10.1364/OE.20.000A85](https://doi.org/10.1364/OE.20.000A85).

- [140] X. Yu, D. Wang, D. Lei, Efficiency improvement of silicon solar cells enabled by zno nanowisker array coating, *Nanoscale Research Letters* 7 (2012). doi:10.1186/1556-276X-7-306.
- [141] Y. Jiang, H. Shen, T. Pu, C. Zheng, Q. Tang, K. Gao, J. Wu, C. Rui, Y. Li, Y. Liu, High efficiency multi-crystalline silicon solar cell with inverted pyramid nanostructure, *Solar Energy* 142 (2017) 91–96. URL: <https://www.sciencedirect.com/science/article/pii/S0038092X16306041>. doi:<https://doi.org/10.1016/j.solener.2016.12.007>.
- [142] S. Kim, J. Park, P. D. Phong, C. Shin, S. M. Iftiqar, J. Yi, Improving the efficiency of rear emitter silicon solar cell using an optimized n-type silicon oxide front surface field layer, *Scientific Reports* 8 (2018). doi:<https://doi.org/10.1038/s41598-018-28823-x>.
- [143] L. Yang, Y. Liu, Y. Wang, W. Chen, Q. Chen, J. Wu, A. Kuznetsov, X. Du, 18.87%-efficient inverted pyramid structured silicon solar cell by one-step cu-assisted texturization technique, *Solar Energy Materials and Solar Cells* 166 (2017) 121–126. URL: <https://www.sciencedirect.com/science/article/pii/S0927024817301307>. doi:<https://doi.org/10.1016/j.solmat.2017.03.017>.
- [144] F. Schindler, A. Fell, R. Müller, J. Benick, A. Richter, F. Feldmann, P. Krenckel, S. Riepe, M. C. Schubert, S. W. Glunz, Towards the efficiency limits of multicrystalline silicon solar cells, *Solar Energy Materials and Solar Cells* 185 (2018) 198–204. URL: <https://www.sciencedirect.com/science/article/pii/S0927024818302186>. doi:<https://doi.org/10.1016/j.solmat.2018.05.006>.
- [145] J. Xu, C. Chen, C. Liu, J. Chen, Z. Liu, X. Yuan, H. Li, High efficiency topcon solar cells with micron/nanostructured emitter for a balance of light-trapping and surface passivation, *Solar Energy Materials and Solar Cells* 238 (2022) 111606. URL: <https://www.sciencedirect.com/science/article/pii/S0927024822000307>. doi:<https://doi.org/10.1016/j.solmat.2022.111606>.
- [146] D. Chen, Y. Chen, Z. Wang, J. Gong, C. Liu, Y. Zou, Y. He, Y. Wang, L. Yuan, W. Lin, R. Xia, L. Yin, X. Zhang, G. Xu, Y. Yang, H. Shen, Z. Feng, P. P. Altermatt, P. J. Verlinden, 24.58% area industrial silicon solar cells with the tunnel oxide passivated contacts (i-topcon) design, *Solar Energy Materials and Solar Cells* 206 (2020) 110258. URL: <https://www.sciencedirect.com/science/article/pii/S0927024819305872>. doi:<https://doi.org/10.1016/j.solmat.2019.110258>.
- [147] H. Hannebauer, T. Dullweber, U. Baumann, T. Falcon, R. Brendel, 21.2% efficient fineline-printed perc solar cell with 5 busbar front grid, *physica status solidi (RRL) – Rapid Research Letters* 8 (2014) 675–679. URL: <https://onlinelibrary.wiley.com/doi/abs/10.1002/pssr.201409190>. doi:<https://doi.org/10.1002/pssr.201409190>. arXiv:<https://onlinelibrary.wiley.com/doi/pdf/10.1002/pssr.20140>
- [148] R. Preu, E. Lohmüller, S. Lohmüller, P. Saint-Cast, J. M. Greulich, Passivated emitter and rear cell—devices, technology, and modeling, *Applied Physics Reviews* 7 (2020) 041315. URL: <https://doi.org/10.1063/5.0005090>. doi:10.1063/5.0005090. arXiv:<https://doi.org/10.1063/5.0005090>.
- [149] M. J. Hossain, M. Sun, G. Doerk, P. G. Kik, K. O. Davis, Self-assembled multifunctional nanostructures for surface passivation and photon management in silicon photovoltaics, *Nanophotonics* 10 (2021) 4611–4621. URL: <https://doi.org/10.1515/nanoph-2021-0472>. doi:10.1515/nanoph-2021-0472.
- [150] F. Feldmann, M. Bivour, C. Reichel, M. Hermle, S. W. Glunz, Passivated rear contacts for high-efficiency n-type si solar cells providing high interface passivation quality and excellent transport characteristics, *Solar Energy Materials and Solar Cells* 120 (2014) 270–274. URL: <https://www.sciencedirect.com/science/article/pii/S0927024813004868>. doi:<https://doi.org/10.1016/j.solmat.2013.09.017>.
- [151] C. Donolato, Effective diffusion length of multicrystalline solar cells, *Semiconductor Science and Technology* 13 (1998) 781. URL: <https://dx.doi.org/10.1088/0268-1242/13/7/021>. doi:10.1088/0268-1242/13/7/021.
- [152] M. J. Hossain, B. Tiwari, I. Bhattacharya, Novel high efficiency quadruple junction solar cell with current matching and quantum efficiency simulations, *Solar Energy* 139 (2016) 100–107. URL: <https://www.sciencedirect.com/science/article/pii/S0038092X16304376>. doi:<https://doi.org/10.1016/j.solener.2016.09.031>.
- [153] P. Wuřfel, T. Trupke, T. Puzzer, E. Schřaffer, W. Warta, S. W. Glunz, Diffusion lengths of silicon solar cells from luminescence images, *Journal of Applied Physics* 101 (2007) 123110. URL: <https://doi.org/10.1063/1.2749201>. arXiv:<https://doi.org/10.1063/1.2749201>. doi:10.1063/1.2749201.
- [154] R. A. Pala, A. J. Leenheer, M. Lichterman, H. A. Atwater, N. S. Lewis, Measurement of minority-carrier diffusion lengths using wedge-shaped semiconductor photoelectrodes, *Energy Environ. Sci.* 7 (2014) 3424–3430. URL: <http://dx.doi.org/10.1039/C4EE01580K>. doi:10.1039/C4EE01580K.
- [155] J. Grandidier, D. M. Callahan, J. N. Munday, H. A. Atwater, Light absorption enhancement in thin-film solar cells using whispering gallery modes in dielectric nanospheres, *Advanced Materials* 23 (2011) 1272–1276. URL: <https://onlinelibrary.wiley.com/doi/abs/10.1002/adma.201004393>. doi:<https://doi.org/10.1002/adma.201004393>. arXiv:<https://onlinelibrary.wiley.com/doi/pdf/10.1002/adma.201>
- [156] Y. Yao, J. Yao, V. K. Narasimhan, Z. Ruan, C. Xie, S. Fan, Y. Cui, Broadband light management using low-q whispering gallery modes in spherical nanoshells, *Nature communications* 3 (2012) 664. doi:10.1038/ncomms1664.
- [157] D. Kray, M. Hermle, S. W. Glunz, Theory and experiments on the back side reflectance of silicon wafer solar cells, *Progress in Photovoltaics: Research and Applications* 16 (2008) 1–15.
- [158] K. O. Davis, K. Jiang, C. Demberger, H. Zunft, H. Haverkamp, D. Habermann, W. V. Schoenfeld, Investigation of the internal back reflectance of rear-side dielectric stacks for c-si solar cells, *IEEE Journal of Photovoltaics* 3 (2013) 641–648.
- [159] Pv lighthouse: Sunsolve, ??? URL: <https://www.pvlighthouse.com.au/sunsolve>.
- [160] Z. C. Holman, M. Filipič, B. Lipovšek, S. De Wolf, F. Smole, M. Topič, C. Ballif, Parasitic absorption in the rear reflector of a silicon solar cell: Simulation and measurement of the subbandgap reflectance for common dielectric/metal reflectors, *Solar Energy Materials and Solar Cells*

- [161] Z. C. Holman, M. Filipič, A. Descoeurdes, S. De Wolf, F. Smole, M. Topič, C. Ballif, Infrared light management in high-efficiency silicon heterojunction and rear-passivated solar cells, *Journal of Applied Physics* 113 (2013) 013107. URL: <https://doi.org/10.1063/1.4772975>. doi:10.1063/1.4772975. arXiv:<https://doi.org/10.1063/1.4772975>.
- [162] Y. Zou, X. Sheng, K. Xia, H. Fu, J. Hu, Parasitic loss suppression in photonic and plasmonic photovoltaic light trapping structures, *Opt. Express* 22 (2014) A1197–A1202. URL: <http://www.opticsexpress.org/abstract.cfm?URI=oe-22-104-A1197>. doi:10.1364/OE.22.0A1197.
- [163] Y. Liu, T. Lai, H. Li, Y. Wang, Z. Mei, H. Liang, Z. Li, F. Zhang, W. Wang, A. Y. Kuznetsov, X. Du, Nanostructure formation and passivation of large-area black silicon for solar cell applications, *Small* 8 (2012) 1392–1397. URL: <https://onlinelibrary.wiley.com/doi/abs/10.1002/sml.201101792>. doi:<https://doi.org/10.1002/sml.201101792>. arXiv:<https://onlinelibrary.wiley.com/doi/pdf/10.1002/sml.20110>
- [164] P. Repo, A. Haarhiltunen, L. Sainiemi, M. Yli-Koski, H. Talvitie, M. C. Schubert, H. Savin, Effective passivation of black silicon surfaces by atomic layer deposition, *IEEE Journal of Photovoltaics* 3 (2013) 90–94. doi:10.1109/JPHOTOV.2012.2210031.
- [165] W.-C. Wang, M.-C. Tsai, J. Yang, C. Hsu, M.-J. Chen, Efficiency enhancement of nanotextured black silicon solar cells using al₂O₃/tio₂ dual-layer passivation stack prepared by atomic layer deposition, *ACS Applied Materials & Interfaces* 7 (2015) 10228–10237. URL: <https://doi.org/10.1021/acsami.5b00677>. doi:10.1021/acsami.5b00677. arXiv:<https://doi.org/10.1021/acsami.5b00677>, PMID: 25919200.
- [166] P. K. Parashar, S. A. Kinnunen, T. Sajavaara, J. J. Toppari, V. K. Komarala, Effective suppression of nanotextured black silicon surface recombination channels by aluminum oxide: comparison from sputtered and ALD grown films, *Semiconductor Science and Technology* 36 (2021) 115013. URL: <https://doi.org/10.1088/1361-6641/ac2124>. doi:10.1088/1361-6641/ac2124.
- [167] X. Liu, B. Radfar, K. Chen, T. P. Pasanen, V. V`ah`anissi, H. Savin, Tailoring femtosecond-laser processed black silicon for reduced carrier recombination combined with >95% above-bandgap absorption, *Advanced Photonics Research* n/a (????) 2100234. URL: <https://onlinelibrary.wiley.com/doi/abs/10.1002/adpr.202100234>. doi:<https://doi.org/10.1002/adpr.202100234>. arXiv:<https://onlinelibrary.wiley.com/doi/pdf/10.1002/adpr.2021>
- [168] H. Heidarzadeh, A. Rostami, M. Dolatyari, G. Rostami, Plasmon-enhanced performance of an ultrathin silicon solar cell using metal-semiconductor core-shell hemispherical nanoparticles and metallic back grating, *Appl. Opt.* 55 (2016) 1779–1785. URL: <http://opg.optica.org/ao/abstract.cfm?URI=ao-55-7-1779>. doi:10.1364/AO.55.001779.
- [169] F. Zhao, J. Lin, Z. Lei, Z. Yi, F. Qin, J. Zhang, L. Liu, X. Wu, W. Yang, P. Wu, Realization of 18.97% theoretical efficiency of 0.9 m thick c-si/zno heterojunction ultrathin-film solar cells via surface plasmon resonance enhancement, *Phys. Chem. Chem. Phys.* 24 (2022) 4871–4880. URL: <http://dx.doi.org/10.1039/D1CP05119A>. doi:10.1039/D1CP05119A.
- [170] M. Wang, H. He, C. Shou, H. Cui, D. Yang, L. Wang, Anti-reflection effect of large-area zno nano-needle array on multi-crystalline silicon solar cells, *Materials Science in Semiconductor Processing* 138 (2022) 106299. URL: <https://www.sciencedirect.com/science/article/pii/S1369800121006338>. doi:<https://doi.org/10.1016/j.mssp.2021.106299>.
- [171] J. Zhu, D. Hu, Y. Wang, C. Tao, H. Jia, W. Zhao, Efficient light trapping from nanorod-like single-textured al-doped zno transparent conducting films, *Coatings* 11 (2021). URL: <https://www.mdpi.com/2079-6412/11/5/513>.
- [172] S. Saravanan, R. Dubey, Performance enhancement of amorphous silicon solar cell using 1d photonic crystal as back reflector, *Materials Today: Proceedings* 49 (2022) 2822–2825. URL: <https://www.sciencedirect.com/science/article/pii/S2214785321064701>. doi:<https://doi.org/10.1016/j.matpr.2021.09.536>, indo-UK International Virtual Conference on Advanced Nanomaterials for Energy and Environmental Applications (ICANEE-2020).
- [173] M. J. Hossain, N. Iqbal, G. Doerk, K. O. Davis, Enhanced light trapping in carrier selective solar cells using photonic nanostructures, in: B. Panchapakesan, A.-J. Attias (Eds.), *Nanoengineering: Fabrication, Properties, Optics, Thin Films, and Devices XVI*, volume 11089, International Society for Optics and Photonics, SPIE, 2019, p. 110890P. URL: <https://doi.org/10.1117/12.2528984>. doi:10.1117/12.2528984.
- [174] M. A. Shameli, P. Salami, L. Yousefi, Light trapping in thin film solar cells using a polarization independent phase gradient metasurface, *Journal of Optics* 20 (2018) 125004. URL: <https://doi.org/10.1088/2040-8986/aaea54>. doi:10.1088/2040-8986/aaea54.
- [175] P. Dhawan, M. Gaudig, A. Sprafke, R. B. Wehrspohn, C. Rockstuhl, Light-trapping structures for planar solar cells inspired by transformation optics, *Opt. Express* 29 (2021) 19903–19919. URL: <http://opg.optica.org/oe/abstract.cfm?URI=oe-29-13-19903>. doi:10.1364/OE.426712.
- [176] M. Sun, P. G. Kik, Scale dependent performance of metallic light-trapping transparent electrodes, *Opt. Express* 28 (2020) 18112–18121. URL: <http://opg.optica.org/oe/abstract.cfm?URI=oe-28-12-18112>. doi:10.1364/OE.391351.
- [177] M. Sun, P. G. Kik, Light trapping transparent electrodes with a wide-angle response, *Opt. Express* 29 (2021) 24989–24999. URL: <https://opg.optica.org/oe/abstract.cfm?URI=oe-29-16-24989>. doi:10.1364/OE.431530.
- [178] M. Sun, P. Golvari, S. M. Kuebler, P. G. Kik, Experimental demonstration of light-trapping transparent electrode geometries, *ACS Photonics* 10 (2023) 595–600. URL: <https://doi.org/10.1021/acsp Photonics.2c01468>. doi:10.1021/acsp Photonics.2c01468. arXiv:<https://doi.org/10.1021/acsp Photonics.2c01468>.
- [179] M. Q. Khokhar, S. Q. Hussain, M. A. Zahid, D. P. Pham, E.-C. Cho, J. Yi, Numerical simulation and experiment of a high-efficiency tunnel oxide passivated contact (topcon) solar cell using a crystalline nanostructured silicon-based layer, *Applied Sciences* 12 (2022). URL: <https://www.mdpi.com/2076-3417/12/1/392>. doi:10.3390/app12010392.
- [180] M. J. Hossain, SunSolve Reflectance EQE J (2023). URL: <https://figshare.com/articles/dataset/SunSolve Reflectance EQE J/23573409.v1>. doi:10.6084/m9.figshare.23573409.v1.